



A global surface CO₂ flux dataset (2015–2022) inferred from OCO-2 retrievals using the GONGGA inversion system

Zhe Jin^{1,2}, Xiangjun Tian^{1,3}, Yilong Wang¹, Hongqin Zhang⁴, Min Zhao¹, Tao Wang¹, Jinzhi Ding¹, Shilong Piao^{1,2,1}

5 ¹State Key Laboratory of Tibetan Plateau Earth System, Resources and Environment (TPESRE), Institute of Tibetan Plateau Research, Chinese Academy of Sciences, Beijing, 100101, China

²Institute of Carbon Neutrality, College of Urban and Environmental Sciences, Peking University, Beijing, 100871, China

³University of Chinese Academy of Sciences, Beijing, 101408, China

⁴Institute of Atmospheric Physics, Chinese Academy of Sciences, Beijing, 100029, China

10 Correspondence to: Xiangjun Tian (tianxj@itpcas.ac.cn) and Yilong Wang (wangyilong@itpcas.ac.cn)



Abstract. Accurate assessment of the size and distribution of carbon dioxide (CO_2) sources and sinks is important for efforts to understand the carbon cycle and support policy decisions regarding climate mitigation actions. Satellite retrievals of the column-averaged dry-air mole fractions of CO_2 (XCO_2) have been widely used to infer spatial and temporal variations of carbon fluxes through atmospheric inversion techniques. In this study, we present a global spatially resolved terrestrial and ocean carbon flux dataset for 2015–2022. The dataset was generated by the Global ObservatioN-based system for monitoring Greenhouse GAses (GONGGA) atmospheric inversion system through the assimilation of Orbiting Carbon Observatory 2 (OCO-2) XCO_2 retrievals. We describe the carbon budget, interannual variability, and seasonal cycle for the global scale and a set of TransCom regions. The 8-year mean net biosphere exchange and ocean carbon fluxes were $-2.22 \pm 0.75 \text{ PgC yr}^{-1}$ and $-2.32 \pm 0.18 \text{ PgC yr}^{-1}$, absorbing approximately 23% and 24% of contemporary fossil fuel CO_2 emissions, respectively. The annual mean global atmospheric CO_2 growth rate was $5.17 \pm 0.68 \text{ PgC yr}^{-1}$, which is consistent with the National Oceanic and Atmospheric Administration (NOAA) measurement ($5.24 \pm 0.59 \text{ PgC yr}^{-1}$). Europe has the largest terrestrial sink among the 11 TransCom land regions, followed by Boreal Asia and Temperate Asia. The dataset was evaluated by comparing posterior CO_2 simulations with the observations from Total Carbon Column Observing Network (TCCON) and Observation Package (ObsPack). Compared with CO_2 simulations using the unoptimized fluxes, the bias and root mean square error of posterior CO_2 simulations were largely reduced across the full range of locations, confirming that the GONGGA system improves the estimates of spatial and temporal variations in carbon fluxes by assimilating OCO-2 XCO_2 data. This dataset will improve the broader understanding of global carbon cycle dynamics and their response to climate change. The dataset can be accessed at <https://doi.org/10.5281/zenodo.8368846> (Jin et al., 2023a).

30

Keywords: global carbon cycle, atmospheric CO_2 , atmospheric inversion, CO_2 fluxes, Observing Carbon Observatory 2, interannual variability, seasonal cycle

35



1 Introduction

Atmospheric carbon dioxide (CO_2) concentrations are rapidly rising, mainly because of increases in anthropogenic emissions. Land and oceans can absorb substantial amounts of CO_2 and thus mitigate global warming. During the past decade (2012–2021), approximately one fourth of total CO_2 emissions were absorbed by the land and oceans, respectively (Friedlingstein et al., 2022). However, there are large uncertainties in estimates of the size, spatial distribution, and interannual variability of land and ocean fluxes (Piao et al., 2009b; Eldering et al., 2017; Hauck et al., 2020; Piao et al., 2020). Accurate estimates of these fluxes at global and regional scales are essential for improving overall knowledge regarding the current status of the carbon cycle and projecting long-term changes (Zscheischler et al., 2017).

There are many methods for the estimation of global and regional carbon budgets, including the inventory method, the eddy covariance method, the ecosystem process modelling method, and the atmospheric inversion method (Piao et al., 2022). The first three methods upscale the site-level ground observations using statistical or process-based models; they are usually regarded as bottom-up approaches. In contrast, atmospheric inversion infers carbon fluxes by combining information from atmospheric CO_2 concentrations, prior flux estimates, and atmospheric transport (Bousquet et al., 2000; Gurney et al., 2002), which is regarded as a top-down approach. Atmospheric inversion is appropriate for assessments of global and regional carbon fluxes because spatiotemporal variations in atmospheric CO_2 concentrations contain the signatures of sources and sinks at large spatial scales. However, inversion accuracy is limited by the numbers and distributions of atmospheric CO_2 observations, uncertainties regarding the atmospheric transport model and the CO_2 emission inventories (such as fossil fuel combustion emissions), and insufficient knowledge of prior flux uncertainties (Liu et al., 2021; Piao et al., 2022).

Currently, atmospheric inversions use either ground-based or space-based observations. Ground-based in situ and flask observations have higher precision, but they are unevenly distributed. Most ground-based observations are mainly concentrated in North America and Europe (Peters et al., 2007; Chevallier et al., 2010; Lauvaux et al., 2016). Inversions using in situ and flask observations can consistently constrain surface CO_2 fluxes at the global scale and at some regional scales (for well-sampled continents), but their uncertainty rapidly increases at the sub-continental scale or when considering continents with sparse observations (Peylin et al., 2013; Byrne et al., 2017; Crowell et al., 2019). For example, there are only eight sites in the Chinese mainland under the World Meteorological Organization/Global Atmosphere Watch program (Wang et al., 2020), and Chinese land sinks constrained by in situ CO_2 observations can differ by up to an order of magnitude (Chen, 2021; Wang et al., 2022a; Wang et al., 2022b). The space-based column-averaged CO_2 dry-air mole fraction (XCO_2) retrievals serve as an emerging data stream for atmospheric inversions. Satellite XCO_2 retrievals have broader spatial coverage than in situ and flask observations; accordingly, they fill observational gaps over areas with few stations. The two most widely used satellites dedicated to measure CO_2 are Greenhouse gases Observing SATellite (GOSAT) (Yokota et al., 2009) and Orbiting Carbon Observatory 2 (OCO-2) (Crisp et al., 2004). GOSAT retrievals have been used in multiple inversions and were shown to be able to reduce the uncertainty of flux estimates in regions where surface CO_2 observations are sparse (Takagi et al., 2011; Basu et al., 2013; Chevallier et al., 2014). The OCO-2 team updates satellite



retrievals roughly once per year. Refinements of instrument error characterization, retrieval algorithms, and bias correction
70 procedures have led to substantial improvements in the accuracy and precision of satellite-retrieved XCO₂ data through these updates (O'dell et al., 2018; Kiel et al., 2019); the single sounding random error of official OCO-2 retrievals is now better than 1 ppm (Eldering et al., 2017; Wunch et al., 2017). These improvements in XCO₂ retrievals have a transformative effect on satellite-based estimates of global carbon fluxes (O'dell et al., 2018; Miller and Michalak, 2020). For example, the OCO-2 version 7 retrievals—the basis of early inversion studies using OCO-2 data—are fit to constrain land carbon fluxes at
75 continental and hemispheric scales (Miller et al., 2018; Crowell et al., 2019). Chevallier et al. (2019) showed that the OCO-2 version 9 retrievals have similar performance in terms of constraining carbon fluxes to the inversions that use observations from surface stations when the inverted fluxes and CO₂ concentrations are compared with independent aircraft data. More recently, the OCO-2 team has released the retrieval product for version 11r. The effectiveness and potential applications of these updated satellite retrievals in efforts to infer surface CO₂ fluxes require continuous and persistent investigation.

80 In this study, we used the GONGGA (Global ObservatioN-based system for monitoring Greenhouse GAses) inversion system (Jin et al., 2023b) to generate a global dataset of terrestrial ecosystem and ocean carbon fluxes from 2015 to 2022 by assimilating OCO-2 XCO₂ retrievals (v11r). Here, we present the prior and posterior global 3-hourly gridded terrestrial ecosystem and ocean carbon fluxes at a spatial resolution of 2° latitude × 2.5° longitude. Gridded fluxes from fossil fuel emissions and biomass burning emissions are also available for inferring the total fluxes.

85 This paper is organized as follows: section 2 describes the methods and data used; section 3 describes the format and content of the dataset; section 4 analyzes the key characteristics of global and regional carbon cycles; section 5 evaluates posterior fluxes using TCCON and ObsPack observations; section 6 introduces data availability; and section 7 summarizes the paper.

2 Methods and Data

90 2.1 The GONGGA inversion system

GONGGA is an atmospheric inversion system that constrains gridded carbon fluxes with atmospheric CO₂ observations and transport simulations (Jin et al., 2023b). The assimilated observations are OCO-2 v11r XCO₂ retrievals (O'dell et al., 2012; O'dell et al., 2018; Gunson and Eldering, 2020), and the transport model is GEOS-Chem v12.9.3 (Suntharalingam et al., 2004; Nassar et al., 2010; Nassar et al., 2013). The spatial resolution of GEOS-Chem is 2° latitude × 2.5° longitude, with 47
95 layers in the vertical direction from the surface to the top of the atmosphere. The model is driven by Modern-Era Retrospective analysis for Research and Applications 2 (MERRA-2) meteorological data provided by the Goddard Earth Observing System (GEOS) of the National Aeronautics and Space Administration (NASA) Global Modeling and Assimilation Office (Gelaro et al., 2017). Four types of carbon fluxes are used to drive the atmospheric CO₂ simulations, including terrestrial ecosystem carbon fluxes (i.e., net ecosystem exchange, NEE), atmosphere-ocean carbon exchange, fossil
100 fuel carbon emissions, and biomass burning carbon emissions. NEE and ocean carbon fluxes are optimized by GONGGA,



whereas fossil fuel emissions and biomass burning emissions are assumed to be well known and not optimized, which is a usual convention in global atmospheric inversions (Peters et al., 2007; Nassar et al., 2011; Crowell et al., 2019; Liu et al., 2021).

GONGGA uses the nonlinear least squares four-dimensional variational data assimilation (NLS-4DVar) method (Tian 105 and Feng, 2015; Tian et al., 2018) to minimize the following cost function:

$$J(\mathbf{x}) = \frac{1}{2}(\mathbf{x} - \mathbf{x}_a)^T \mathbf{B}^{-1} (\mathbf{x} - \mathbf{x}_a) + \frac{1}{2}(\mathbf{y} - h(\mathbf{x}))^T \mathbf{R}^{-1} (\mathbf{y} - h(\mathbf{x})). \quad (1)$$

where \mathbf{x} is the state vector that contains the variables to be optimized and \mathbf{x}_a is its prior estimate, \mathbf{B} is the prior error covariance matrix, \mathbf{y} gathers the XCO₂ retrievals, $h(\cdot)$ is the observation operator, and \mathbf{R} is the observation error covariance matrix. As a hybrid assimilation method, NLS-4DVar combines the advantages of the conventional four-dimensional variational (4D-Var) method and ensemble Kalman filter (EnKF); it can achieve high inversion accuracy with low computational cost and complexity (Tian and Feng, 2015; Tian et al., 2018). GONGGA adopts a novel dual-pass inversion strategy, successively optimizing initial CO₂ concentrations and surface carbon fluxes within each inversion cycle of 14 days; this distinguishes model–data mismatches caused by errors from initial CO₂ concentrations and surface fluxes (Jin et al., 110 2023b). Note that during the flux optimization, the state vector \mathbf{x} gathers gridded scaling factors for NEE and ocean carbon 115 fluxes. In this study, GONGGA was run from September 6, 2014 to December 31, 2022. The 2014 results were regarded as spin-up, whereas the 8-year results spanning 2015–2022 comprised the dataset.

2.2 Prior CO₂ fluxes and uncertainties

The prior CO₂ fluxes include NEE, ocean carbon fluxes, fossil fuel emissions, and biomass burning emissions. The prior NEE was simulated by ORCHIDEE-MICT (Guimbertea et al., 2018). The prior ocean carbon fluxes were from the CT2022 120 *p*CO₂-Clim prior data, which were derived from the Takahashi et al. (2009) climatology of seawater *p*CO₂. Fossil fuel emissions were from the monthly Global Carbon Budget Gridded Fossil Emissions Dataset (GCP-GridFED; version 2023.1) (Jones et al., 2021). Biomass burning emissions were from the Global Fire Emissions Database (GFED, version 4.1s) 0.25° × 0.25° monthly data scaled with daily factors (Randerson et al., 2017; Van Der Werf et al., 2017). For estimation of prior flux 125 uncertainties, we first used a prior perturbation ensemble to approximate the prior scaling factor error covariance matrix, then calculated the prior flux uncertainties through the matrix multiplication between the scaling factor error covariance matrix and prior fluxes. The posterior flux uncertainties were calculated in the same manner, using the ensemble of posterior scaling factors and prior fluxes. The difference between the prior and posterior flux uncertainties was regarded as the difference in perturbation ensemble. For detailed steps, see Text S1 in the Supplement.

2.3 OCO-2 column CO₂ observations

130 We used OCO-2 Level 2 Lite v11r XCO₂ products (O'dell et al., 2012; O'dell et al., 2018; Gunson and Eldering, 2020) retrieved by the Atmospheric Carbon Observations from Space (ACOS) algorithm (Connor et al., 2008) to constrain the



surface carbon fluxes. The OCO-2 satellite carries high-resolution spectrometers that return high-precision measurements of reflected sunlight received within the CO₂ and O₂ bands in the short-wave infrared spectrum (Crisp et al., 2012). The OCO-2 spacecraft flies in a 705-km-altitude sun-synchronous orbit with a 16-day (233 orbits) ground track repeat cycle. OCO-2 has 135 a footprint of 1.29 × 2.25 km² at nadir mode and acquires eight cross-track footprints, creating a swath width of 10.3 km.

Before assimilation, the XCO₂ retrievals were filtered with the xco2_quality_flag parameter provided by the OCO-2 Lite products; xco2_quality_flag = 0 (1) denotes good (bad) retrieval quality. Only retrievals with good quality were selected. Additionally, because the spatial resolution of the transport model is significantly coarser than the spatial resolution of OCO-2 retrievals, observation thinning was performed to reduce sampling error. We set the threshold of the number of daily 140 observations to 20,000. If the number of good retrievals exceeded the threshold within a single day, excess data were removed. For example, if there were 60,000 good retrievals in one day, one of every three sequential retrievals was selected according to sounding ID. Furthermore, to ensure consistency between ground- and satellite-based observations, OCO-2 retrievals were scaled to the official World Meteorological Organization (WMO) X2019 standards, in accordance with instructions provided by the National Oceanic and Atmospheric Administration (NOAA,

145 <https://docs.google.com/document/d/e/2PACX->

<https://docs.google.com/document/d/e/2PACX-1vQ0JqK72fAOThaJwJyILLgfoE2qpHYdgNsIYAs6T2cMGumwVlISK7lurIYKCMOfgz1fyxuKYwlm5FEx/pub>, last access: September 12, 2023).

2.4 Evaluation of posterior fluxes

Generally, it is difficult to directly verify the posterior fluxes because of the lack of direct flux observations that exhibit a 150 footprint size comparable with the spatial resolution of global inversion models (typically several hundred kilometers). Instead, we compared the simulated CO₂ concentrations driven by posterior fluxes with atmospheric CO₂ observations to achieve indirect verification (e.g., Wang et al. (2019); Wu et al. (2020); Liu et al. (2021)). In this study, we performed these comparisons using observations from TCCON and ObsPack.

2.4.1 TCCON XCO₂ retrievals

155 TCCON is a network of ground-based Fourier transform spectrometers that record direct solar spectra in the near-infrared spectral region. From these spectra, accurate and precise column-averaged CO₂ abundances are retrieved and reported (Wunch et al., 2011). TCCON XCO₂ retrievals are estimated to have precisions better than 0.25% (i.e., ~1 ppm) (Wunch et al., 2011). These retrievals have been used as primary validation data for several satellite missions, including GOSAT and OCO-2 (Wunch et al., 2011; Wunch et al., 2017). Here, we used GGG2020 version data (Wunch et al., 2015). There are 27 160 TCCON sites with observations covering the inversion period; the site locations are shown in Figure 1a.

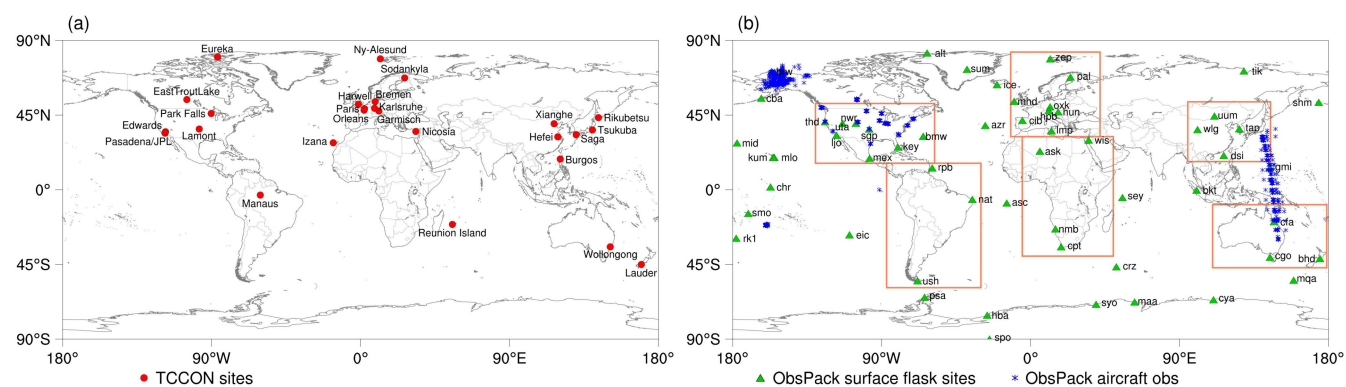


2.4.2 ObsPack CO₂ observations

ObsPack is a framework that combines atmospheric greenhouse gas observations from various sampling platforms (e.g., surface, aircrafts, towers, or ships) and strategies (e.g., flask or in situ), ensuring consistent data quality (Masarie et al., 2014). In this study, we used the surface flask and aircraft observations from obspack_co2_1_GLOBALVIEWplus_v8.0_2022-08-165 27 in 2015–2021 and obspack_co2_1_NRT_v8.1_2023-02-08 in 2022, both of which are established according to the WMOX2019 scale (Cox et al., 2022). Surface flask observations are usually made on a weekly basis. During the 2015–2022 period, surface flask observations from 57 sites with parameter CT_assim = 1 or 2 were used for evaluation (Fig. 1b). Observations may be reported by multiple institutes at a single site. Here, we only used data from the NOAA laboratory and ignored duplicate records from other sites. Based on the spatial distribution of surface flask sites, we evaluated terrestrial 170 carbon fluxes in six regions: North America, South America, Europe, Africa, East Asia, and Australia (Fig. 1b).

Aircraft observations contain data from the Comprehensive Observation Network for TRace gases by AIRLiner (CONTRAIL) program, Carbon in Arctic Reservoirs Vulnerability Experiment (CARVE) program, and several localized measurements concentrated in North America (Fig. 1b). The CONTRAIL program is Japan's unique aircraft observation project that measures atmospheric CO₂ concentrations using instruments onboard Japan Airlines (JAL) commercial airliners.

175 In the ObsPack v8.0 dataset, the CONTRAIL program contains aircraft measurements between Japan and Australia from 2015 to 2021. The CARVE program was a NASA Earth Venture Suborbital-1 mission, which collected airborne measurements of atmospheric CO₂ in the Alaskan Arctic from 2011 to 2015. We used CO₂ observations above the planetary boundary layer (altitude > 1 km) for evaluations to avoid effects on local emissions related to aircraft ascent and descent.



180 **Figure 1. Spatial distributions of (a) TCCON sites and (b) ObsPack sites used for flux evaluations. Rectangles show the ranges of the six regions used for comparisons with surface flask observations.**

3 Dataset description

Here, we present a global dataset that contains surface carbon fluxes from 2015 to 2022. The flux files contain NEE, ocean carbon fluxes, fossil fuel emissions, and biomass burning emissions. The NEE and ocean carbon fluxes include prior and



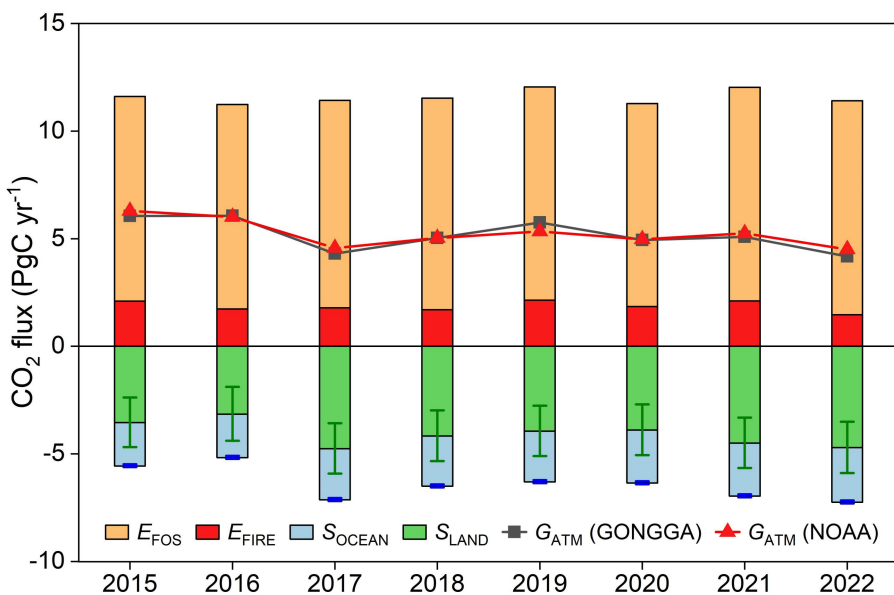
185 posterior estimates. The corresponding gridded uncertainties of NEE and ocean fluxes are also included in the flux files. The global gridded fluxes are 3-hourly with a resolution of 2° latitude $\times 2.5^\circ$ longitude.

4 Results

4.1 Global carbon budget

Here, we quantify the five major components of the global carbon budget, including the fossil fuel CO₂ emissions (E_{FOS}), 190 biomass burning emissions (E_{FIRE}), atmospheric CO₂ concentration growth rate (G_{ATM}), ocean CO₂ sink (S_{OCEAN}), and terrestrial CO₂ sink (S_{LAND}) (Fig. 2); in this paper, S_{LAND} refers to NEE. During the 2015–2022 period, E_{FOS} was 9.71 ± 0.20 PgC yr⁻¹, with a minimum of 9.44 PgC yr⁻¹ in 2020 and a maximum of 9.94 PgC yr⁻¹ in 2022; E_{FIRE} was 1.86 ± 0.22 PgC yr⁻¹, with a minimum of 1.47 PgC yr⁻¹ in 2022 and a maximum of 2.14 PgC yr⁻¹ in 2019. Over this 8-year period, NEE had substantial interannual variability (-4.08 ± 0.53 PgC yr⁻¹); the sinks were significantly weaker in 2015 and 2016 than in 195 other years. The annual mean NEE in 2015–2016 was -3.35 PgC yr⁻¹, whereas the NEE in 2017–2022 was -4.33 PgC yr⁻¹. The reduced terrestrial carbon sink was mainly related to the El Niño event during 2015–2016, which caused substantial carbon release in the tropics (Wang et al., 2013; Liu et al., 2017; Piao et al., 2020; Dannenberg et al., 2021). Compared with NEE, interannual variation in the ocean sink was much smaller (-2.32 ± 0.18 PgC yr⁻¹). From 2015 to 2022, the terrestrial biosphere ($S_{\text{LAND}}+E_{\text{FIRE}}$) and ocean absorbed approximately 23% and 24% of total fossil fuel CO₂ emissions, respectively, 200 resulting in a G_{ATM} of 5.17 ± 0.68 PgC yr⁻¹.

We compared the GONGGA-estimated global carbon budget with results from the measurements and Global Carbon Budget 2022 (hereafter referred to as GCB2022) (Friedlingstein et al., 2022). The G_{ATM} directly estimated from atmospheric CO₂ concentration measurements provided by the NOAA Earth System Research Laboratories Global Monitoring Laboratory (ESRL/GML) was 5.24 ± 0.59 PgC yr⁻¹ during 2015–2022 (Dlugokencky and Tans, 2022), which corroborates 205 the GONGGA estimate. We also compared net biosphere exchange (NBE, the net carbon flux of all the land – atmosphere exchange processes except fossil fuel emissions) and ocean fluxes from the GONGGA inversion and GCB2022 for the period 2015–2021, as GCB 2022 does not contain data for 2022. Note that the GCB2022 estimated land and ocean sinks are from process models (Friedlingstein et al., 2022). While comparing GONGGA inversion results with the process models of GCB2022, lateral carbon transport through the land–ocean aquatic continuum (LOAC) of 0.65 ± 0.35 PgC yr⁻¹ (Regnier et 210 al. (2022) was adjusted to ensure the consistency between bottom-up and top-down methods. The adjusted mean NBE from GONGGA during 2015–2021 was -1.42 ± 0.53 PgC yr⁻¹, and the mean ocean sink was -2.94 ± 0.17 PgC yr⁻¹, which were within the range of the results from GCB2022 (NBE: -1.38 ± 0.65 PgC yr⁻¹; S_{OCEAN} : -2.93 ± 0.06 PgC yr⁻¹).



215 **Figure 2. Global carbon budget estimated by GONGGA and atmospheric CO₂ growth rate from NOAA during 2015–2022.**

4.2 Global distribution and regional fluxes

Figure 3 shows the global distributions of GONGGA annual mean NBE and ocean carbon fluxes during 2015–2022. Terrestrial carbon sinks were mainly in temperate North America, central South America, southern Africa, Europe, boreal 220 Asia, India, eastern China, and most of Australia. Terrestrial carbon sources mainly occurred over western America, the eastern Amazon, central Africa, Southeast Asia, the southeastern coast of Australia, and New Zealand. The ocean sources mainly occurred over tropical oceans and the high-latitude Southern Ocean; the equatorial Pacific was the most prominent source area. Sinks mainly occurred over mid-latitude regions of both hemispheres and the high-latitude northern ocean. Generally, NBE had a more complex spatial distribution and higher uncertainty, compared with ocean carbon fluxes. 225 Therefore, we explored the distribution and attribution of NBE over 11 TransCom land regions (Fig. 4) (Gurney et al., 2004).

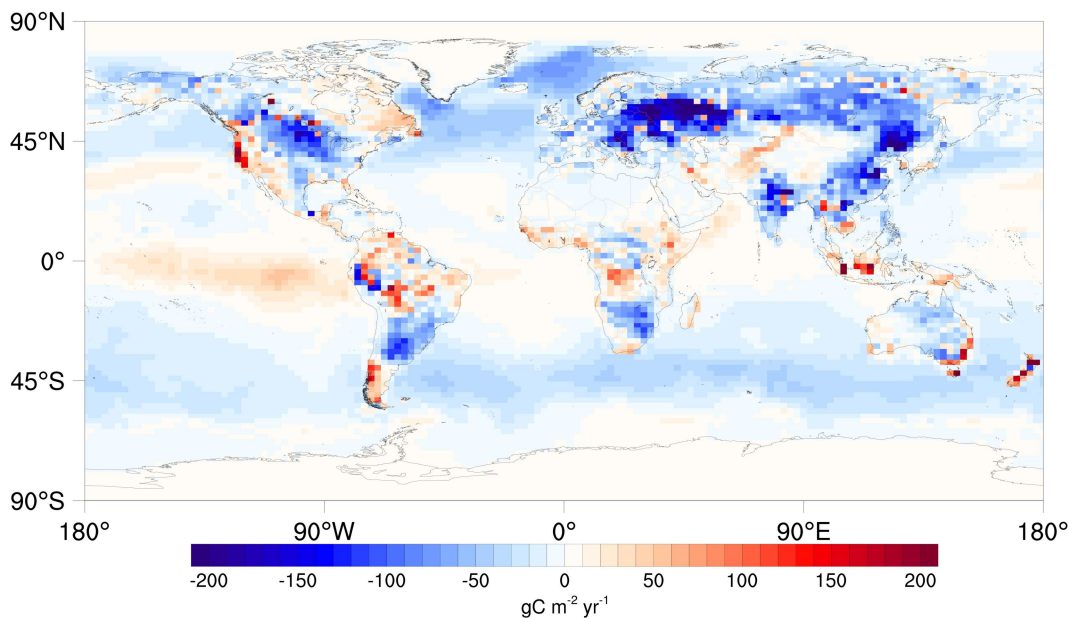
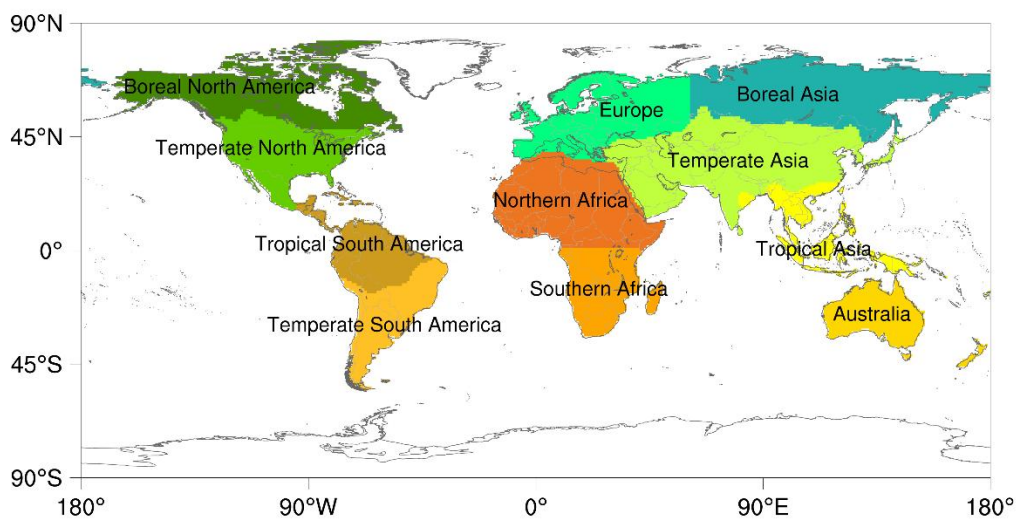


Figure 3. GONGGA-estimated global distributions of annual mean (2015–2022) NBE and ocean carbon fluxes.



230 **Figure 4. Spatial distributions of 11 TransCom land regions.**

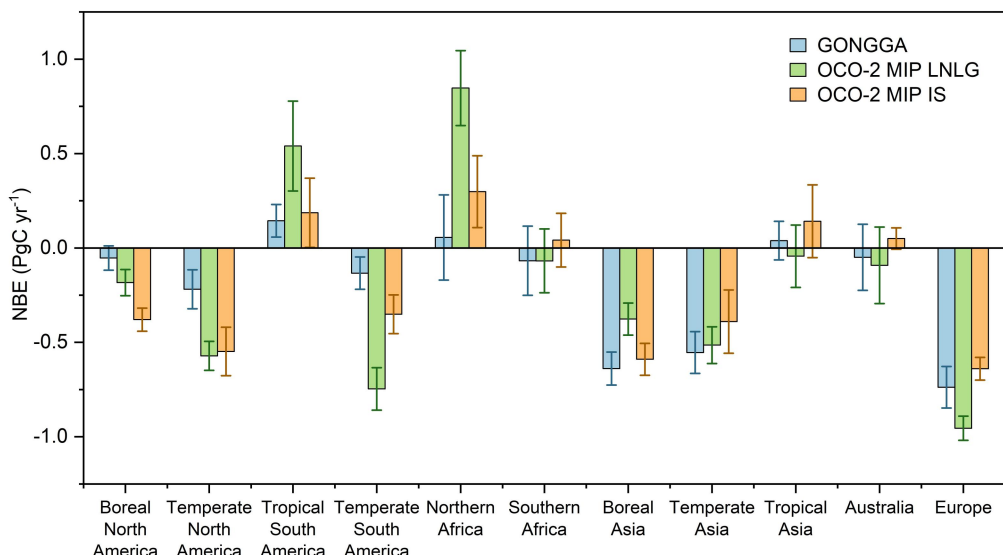
Here, we present the GONGGA-estimated annual mean (2015–2022) NBE for 11 TransCom land regions and their comparison with OCO-2 model intercomparison project (MIP) v10 inversions (Fig. 5). OCO-2 MIP v10 (Crowell et al., 2019; Peiro et al., 2022) includes an ensemble of 14 atmospheric inversions using the same set of OCO-2 v10r retrievals and observation uncertainties for the period of 2015–2020, each of which is characterized by distinct transport models, data assimilation algorithms, and prior fluxes (Table S1). We used OCO-2 MIP v10 results from the inversions that assimilate



land nadir and land glint (LNLG) satellite retrievals, and those assimilate in situ (IS) measurements. Here, in situ inversions are used to provide a baseline against satellite-driven results.

For the 11 TransCom regions, we estimated that Europe had the strongest terrestrial carbon sink, followed by Boreal Asia, Temperate Asia, Temperate North America, Temperate South America, Southern Africa, Boreal North America, and 240 Australia, whereas Tropical South America, Northern Africa and Tropical Asia were terrestrial carbon sources. All GONGGA and OCO-2 MIP LNLG and IS consistently indicated that Europe was the largest terrestrial sink. GONGGA showed good agreement with OCO-2 MIP inversions for most regions, and divergences occur mainly in the northern high latitudes and in the equatorial regions (e.g., Boreal North America and Northern Africa). The nearly neutral terrestrial carbon uptake from GONGGA in these regions may be related to the prior NBE adopted and limited number of high-quality OCO-2 245 retrievals. According to the prior estimates, Boreal North America was a net terrestrial carbon source and Northern Africa was a net terrestrial sink during 2015–2022 (Fig. S1), in contrast to the OCO-2 MIP results. After the assimilation of OCO-2 retrievals, the posterior NBE in these two regions were closer to OCO-2 MIP results, but the improvements were limited. These findings were also partly related to the limited constraints from OCO-2 observations. For example, in Boreal North 250 America, satellites cannot measure XCO₂ in dark high-latitude areas in winter. In Northern Africa, OCO-2 also has difficulties in accurately measuring XCO₂ over the desert because of its high albedo, demonstrated by its high proportion of bad retrievals (`xco2_quality_flag = 1`) (Zhang et al., 2016). Therefore, the posterior fluxes in these two regions mirrored the prior fluxes during the time period with few OCO-2 retrievals. Notably, even in OCO-2 MIP inversions, the ensemble spread was prominent, indicating the difficulty of inversion in these regions using current satellite or in situ observations (Table S2).

In Africa, Southern America, Tropical Asia, and Australia, fire emissions significantly contributed to the regional 255 carbon balance (Fig. S2). Accordingly, these regions were either net carbon sources or carbon neutral. In recent decades, ~50% of fire-related carbon emissions and ~70% of global burned areas occurred across African subtropical savannah systems (Giglio et al., 2013; Andela and Van Der Werf, 2014). In the Amazon, the mean gross emissions from forest fires from 2003 to 2015 was 454 ± 496 Tg CO₂ yr⁻¹, which may counteract the decline of Amazon deforestation carbon emissions (Aragão et al., 2018). Southeast Australia experienced intensive and geographically extensive wildfires during the 2019– 260 2020 summer season, and the fires released substantial amounts of CO₂ into the atmosphere (Van Der Velde et al., 2021). These examples show that fire can have substantial negative impacts on the environment and climate (Moritz et al., 2014; Bowman et al., 2017).



265

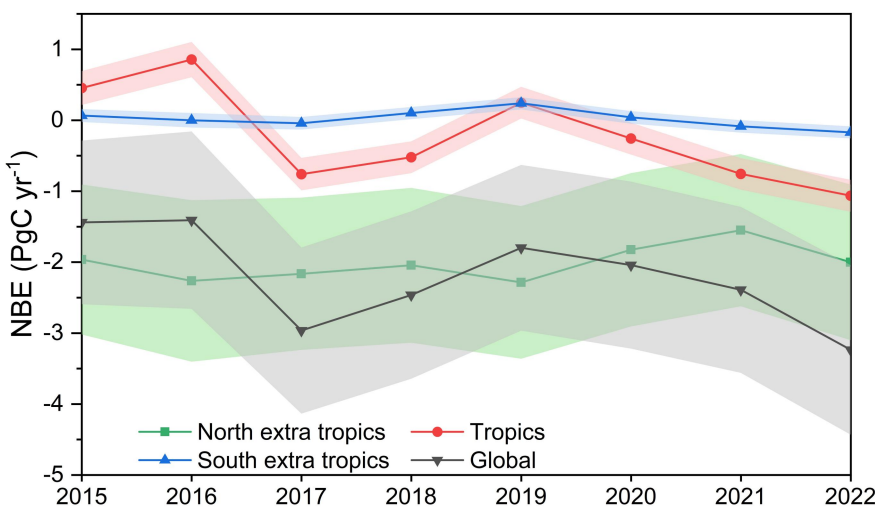
Figure 5. GONGGA annual mean (2015–2022) NBE for 11 TransCom land regions and comparisons with OCO-2 MIP LNLG and IS inversions. Error bars represent standard deviations in annual mean budget across the whole period.

4.3 Interannual variability and seasonal cycle

Here, we analyzed the interannual variability (IAV) and seasonal cycle of NBE at global and regional scales. We divided the globe into three large latitude bands: northern extratropics (30–90°N), tropics (30°S–30°N), and southern extratropics (90–30°S). The global net terrestrial carbon flux has a prominent year-to-year variability (Friedlingstein et al., 2022). We estimated that the magnitude of global NBE IAV was 0.63 PgC yr⁻¹ during the 2015–2022 period. We calculated the contribution of each latitude band to the global IAV using Eq. (1) from Ahlström et al. (2015). The contribution of the tropics to the global NBE IAV was 100.8%, whereas the contributions of the northern and southern extratropics were –13.2% and 12.4%, respectively. A positive (negative) score here indicates the variation is in the same (opposite) phase as the global IAV. The scores from our estimate indicated that the global IAV arises from the tropics. Considering the short time series of the carbon cycle, the latitudinal contributions in this study are qualitative, rather than quantitative. The dominant role of tropical terrestrial ecosystems in the signal of the global carbon cycle IAV is consistent with previous results based on multiple observations and models (Baker et al., 2006; Rödenbeck et al., 2018a, b; Jung et al., 2020). Piao et al. (2020) reviewed and analyzed the regional contribution to global net terrestrial carbon flux IAV from 1980 to 2017 with process-based land carbon cycle models, atmospheric inversion models, and FLUXCOM data products. The contributions of the tropics to the global IAV obtained by these three methods were 83.4%, 71.7%, and 69.7%, respectively. In addition to the short time series, the inclusion of the 2015–2016 strong El Niño event in the period is an important reason for the large contribution score of the tropics in our estimate. Climatic variations are the main factors that drive the IAV of the net terrestrial carbon flux (Braswell et al., 1997; Zeng et al., 2005; Raupach et al., 2008; Liu et al., 2017). El Niño is the major climatic mode that modulates global temperature, precipitation, and solar radiation (Gu and Adler, 2011); thus, it drives the



IAV of the carbon cycle (Bacastow, 1976; Rayner et al., 2008). The characteristics of hot and dry climate conditions in El Niño years are the primary reasons for the lower net carbon uptake or net carbon release by terrestrial ecosystems (Jones et al., 2001; Piao et al., 2009a), which is particularly evident in the tropics (Fig. S3) (Liu et al., 2017; Jin et al., 2023b). During 290 2015–2016, tropical land released 0.66 PgC yr⁻¹ CO₂ into the atmosphere, whereas it is a net terrestrial sink in normal years (~0.52 PgC yr⁻¹).



295 **Figure 6. Interannual variability of NBE over the globe, northern extra-tropics (30–90°N), tropics (30°S–30°N), and southern extra-tropics (90–30°S) during 2015–2022. Shadowed area represents the uncertainty of NBE in each region.**

The shape of the NBE seasonal cycle varies among regions and different years. In the northern extratropics, the size and phase of the seasonal cycle are very similar in all years, with July having the largest sink and northern winter being a carbon source. In the tropics, however, the seasonal cycles are more flatten and are distinct in different years. The largest deviations of the tropical seasonal cycle from the 8-year mean estimate are in 2016 ($R^2 = 0.34$, coefficient of determination between 300 annual mean seasonal cycle and the year investigated) and 2019 ($R^2 = 0.50$); the most prominent deviations occurred during the peak 2015–2016 El Niño between July 2015 and June 2016 as well as 2019 El Niño between April 2019 and July 2019. The shape of the global seasonal cycle is nearly similar to the shape of the northern extratropics (with 103.6% contribution), whereas the tropics and southern extratropics have opposite phases compared with the global seasonal cycle (with -1.1% and -2.5% contribution, respectively). The dominance of the northern extratropics in the global seasonal cycle is consistent with 305 previous findings (Forkel et al., 2016; Piao et al., 2020).

The amplitude is an important index of the seasonal cycle (i.e., seasonal cycle amplitude, SCA). The peak-to-trough amplitude was calculated as the difference between the maximum and minimum monthly NBE in each year. The 8-year mean SCA of NBE for the globe, northern extratropics, tropics, and southern extratropics were 3.55, 3.50, 0.43, and 0.12 PgC month⁻¹, respectively. The larger mean amplitude in northern land ecosystems, compared with other regions, was 310 mainly related to the strong seasonality of gross primary production and ecosystem respiration (Randerson et al., 1997).

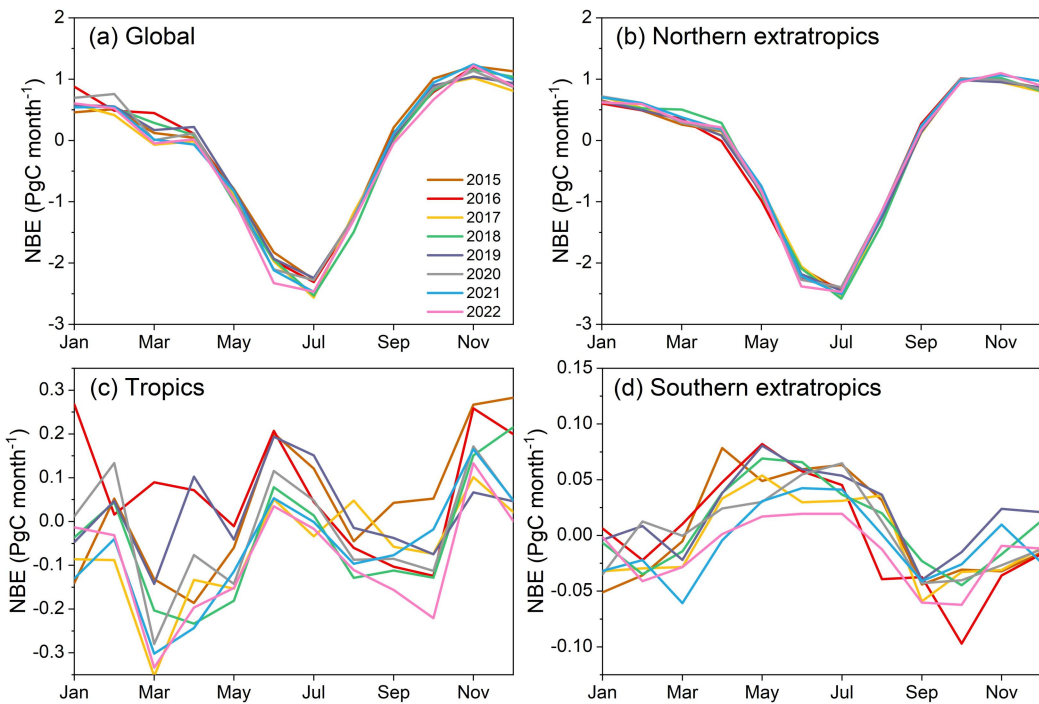


Figure 7. Seasonal cycle of NBE for the globe, northern extratropics, tropics, and southern extratropics during 2015–2022.

5 Dataset evaluation

315 5.1 Comparison with TCCON observations

In this section, we compare the simulated monthly mean XCO₂ driven by the posterior CO₂ fluxes with the observations from 27 TCCON sites during 2015–2022 (Table 1). The global mean root mean square error (RMSE) and BIAS between simulated and observed XCO₂ were 0.81 and 0.24 ppm, respectively. Through the assimilation of OCO-2 retrievals, the atmospheric CO₂ simulations were considerably improved compared with prior simulations, which exhibited 1.15 ppm

320 RMSE and 0.51 ppm BIAS at the global scale. At most sites, posterior RMSE was < 1 ppm, and BIAS was in the range of −0.5 to 1 ppm (Fig. 8). The maximum simulation deviation occurred at Eureka station (unless otherwise stated, “simulations” hereafter refers to posterior simulations), where an overestimation of simulated XCO₂ was observed in winter. This overestimation was also evident at Ny Ålesund and Sodankylä, which are located in the high latitudes of the Northern Hemisphere. Prior simulations generally overestimated CO₂ concentrations, particularly in winter (Fig. S4). Positive 325 deviations were adequately mitigated at most sites after the inversion. However, for the sites mentioned above, considering the lack of satellite retrievals in winter at high northern latitudes, the posterior flux may be poorly constrained and is thus similar to the prior flux. Additionally, the coarse spatial resolution of the transport model is another challenge for the



detection of sub-grid variations in XCO₂. For example, Edwards station and Pasadena station are close to each other; thus, they are located in the same grid cell of the transport model. The simulated XCO₂ time series at these two sites are similar, 330 and the minor difference mainly arises from the interpolation process (Fig. S5). In contrast, the XCO₂ observations are considerably higher at Pasadena station than at Edwards station, with a multi-year mean difference of 0.84 ppm.

Table 1. Geographic locations and references of TCCON sites used for validation. Sites are listed according to latitude from north to south.

Station	Latitude	Longitude	Country	Data Reference
Eureka	80.0	-86.4	Canada	Strong et al. (2022)
Ny Ålesund	78.9	11.9	Norway	Buschmann et al. (2022)
Sodankylä	67.4	26.6	Finland	Kivi et al. (2022)
East Trout Lake	54.4	-105.0	Canada	Wunch et al. (2022)
Bremen	53.1	8.9	Germany	Notholt et al. (2022)
Harwell	51.6	-1.3	United Kingdom	Weidmann et al. (2023)
Karlsruhe	49.1	8.4	Germany	Hase et al. (2022)
Paris	49.0	2.4	France	Té et al. (2014)
Orléans	48.0	2.1	France	Warneke et al. (2022)
Garmisch	47.5	11.1	Germany	Sussmann and Rettinger (2022)
Park Falls	46.0	-90.3	United States	Wennberg et al. (2022d)
Rikubetsu	43.5	143.8	Japan	Morino et al. (2022b)
Xianghe	39.8	117.0	China	Zhou et al. (2022)
Lamont	36.6	-97.5	United States	Wennberg et al. (2022b)
Tsukuba	36.1	140.1	Japan	Morino et al. (2022a)
Nicosia	35.1	33.4	Cyprus	Petri et al. (2022)
Edwards	35.0	-117.9	United States	Iraci et al. (2022)
Jet Propulsion Laboratory	34.2	-118.2	United States	Wennberg et al. (2022a)
Pasadena	34.1	-118.1	United States	Wennberg et al. (2022c)
Saga	33.2	130.3	Japan	Shiomi et al. (2022)
Hefei	31.9	117.2	China	Liu et al. (2022)
Izana	28.3	-16.5	Spain	García et al. (2022)
Burgos	18.5	120.7	Philippines	Morino et al. (2022c)
Manaus	-3.2	-60.6	Brazil	Dubey et al. (2022)



Réunion Island	-20.9	55.5	France	De Mazière et al. (2022)
Wollongong	-34.4	150.9	Australia	Deutscher et al. (2023)
Lauder	-45.0	169.7	New Zealand	Pollard et al. (2022); Sherlock et al. (2022)

335

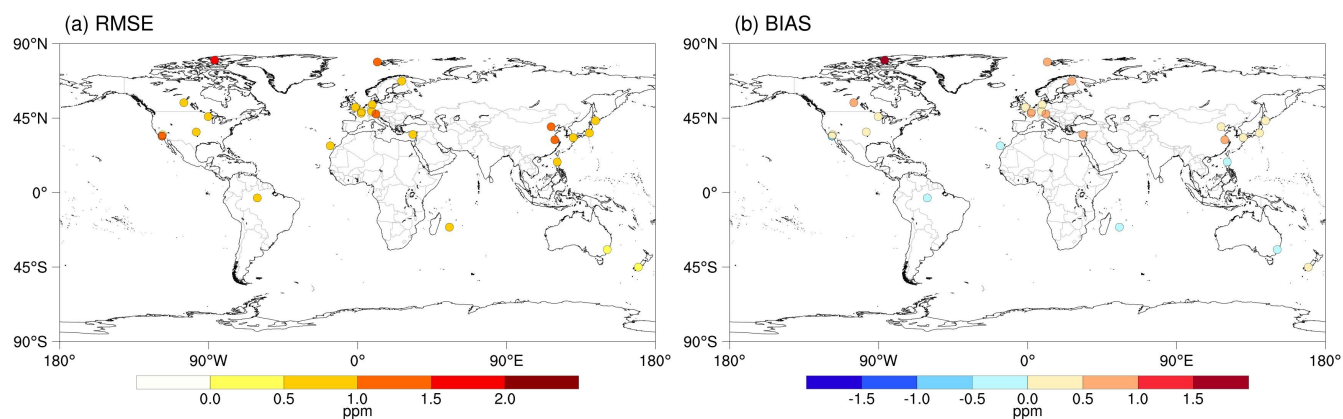
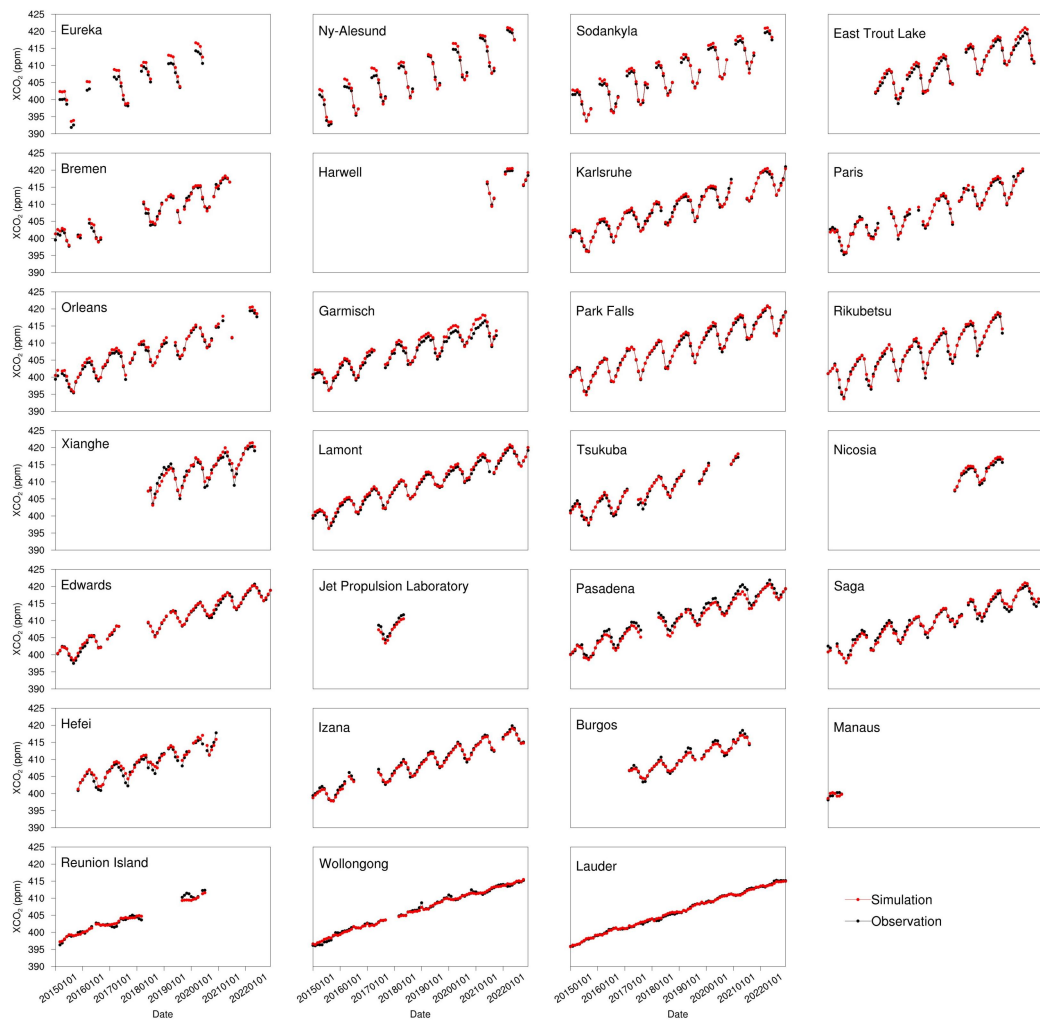


Figure 8. Spatial distributions of (a) root mean square error (RMSE) and (b) BIAS between the posterior monthly XCO₂ simulations and corresponding observations at each TCCON site (simulations minus observations; unit: ppm).



340

Figure 9. Time series of monthly averaged observations and simulations at each TCCON site.

5.2 Comparison with ObsPack observations

Here, we compare posterior CO₂ simulations with ObsPack surface flask and aircraft observations. The global mean RMSE and BIAS between surface flask observations and corresponding simulations were 1.76 and -0.33 ppm, respectively. For 345 most surface flask sites located on the ocean and in tropical and southern extratropical terrestrial regions, RMSE was < 2.0 ppm; BIAS was in the range of -0.5 ppm to 0.5 ppm. The high model–data RMSE values mainly occurred over northern middle latitudes, particularly over Europe and East Asia. Jiang et al. (2022) used GOSAT XCO₂ retrievals to estimate global CO₂ fluxes and also found that posterior CO₂ concentrations could differ from surface observations, mainly in the northern extratropics. Because of limitations regarding the coarse resolutions of global transport models and thus differences in 350 representativeness between simulated CO₂ concentrations and actual observations over land, some sites have significant



data–model mismatches. For example, at the three sites with posterior RMSE values exceeding 4.0 ppm, the observed atmospheric CO₂ concentrations had strong temporal fluctuations, which were presumably caused by localized and short-term surface fluxes (Fig. S6).

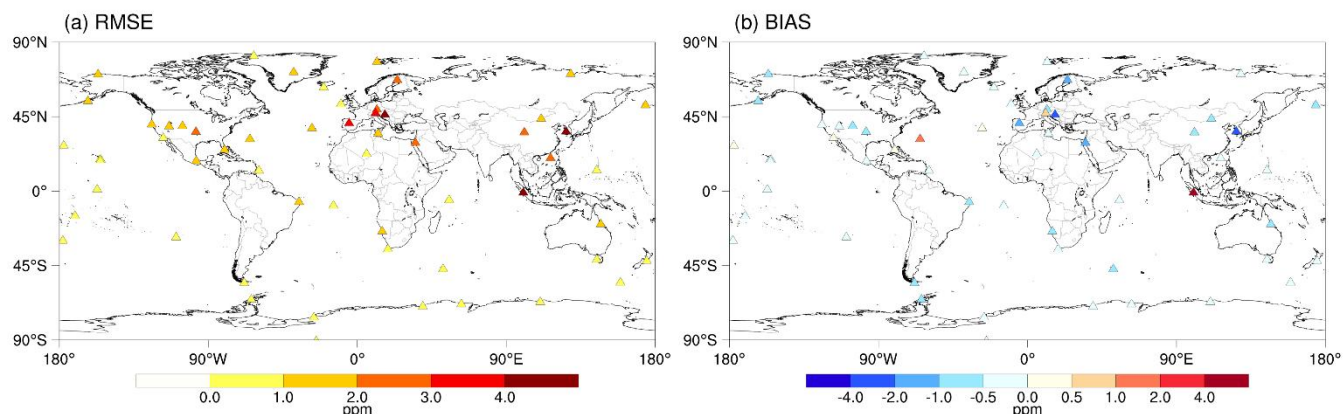
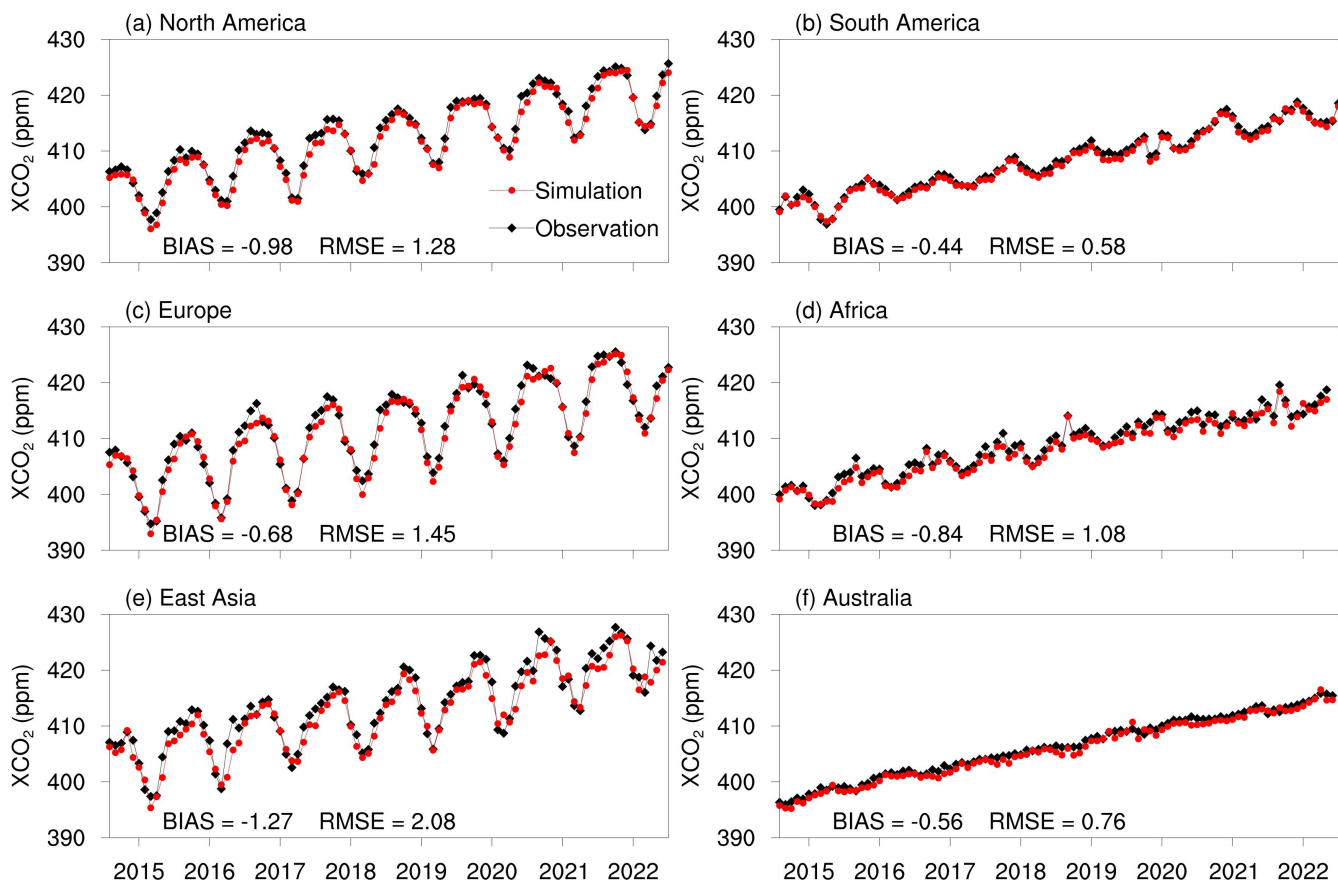


Figure 10. Spatial distributions of (a) RMSE and (b) BIAS between the posterior monthly XCO₂ simulations and corresponding observations at each surface flask site (simulations minus observations; unit: ppm).

355

To decrease mismatches in temporal and spatial representativeness between observations and simulations, we compared the monthly observed and simulated CO₂ concentrations in six land regions (Fig. 11). The monthly simulations closely 360 agreed with the observations; RMSE was in the range of 0.58 to 2.08 ppm, and BIAS was in the range of −0.44 to −1.27 ppm. The simulation deviations remained higher for North America, Europe, and East Asia, compared with other regions. In these 365 three regions, there was a significant difference in terms of comparisons with TCCON and ObsPack surface flask observations; mainly positive BIAS arose from TCCON evaluations and negative BIAS arose from ObsPack evaluations. This discrepancy may be related to the nature of the two types of observations. TCCON observations are column-averaged 370 atmospheric CO₂ concentrations, whereas ObsPack observations are surface atmospheric CO₂ concentrations. The opposite signs of BIAS between the two comparisons may be related to the imperfect simulation of vertical mixing of GEOS-Chem (Schuh et al., 2019).



370 **Figure 11. Time series of monthly averaged ObsPack surface flask observations and corresponding simulations for the six sub-regions.**

375 For aircraft observations, we calculated the mean statistics of each grid cell (Fig. 12). The simulations closely agreed with the aircraft observations. For most grid cells, the RMSE was < 2.0 ppm; bias was between –1.0 and 1.0 ppm. The simulated deviations over Alaska and Temperate North America were generally larger than over the ocean, similar to the surface flask results.

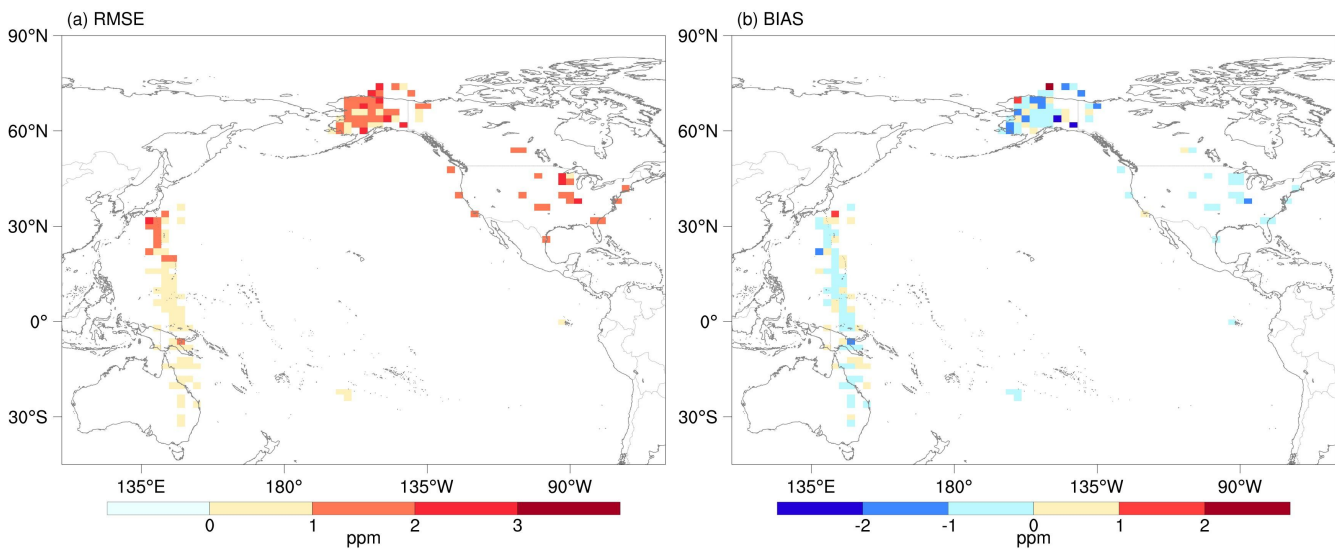


Figure 12. The (a) BIAS and (b) RMSE between posterior CO₂ and aircraft observations at each grid cell (simulations minus observations; unit: ppm).

380 6 Data availability

The dataset is available at <https://doi.org/10.5281/zenodo.8368846> (Jin et al., 2023a). As the satellite XCO₂ retrievals, prior carbon fluxes, and meteorological data are persistently improving and updating, we plan to update the dataset annually in the future, aiming to support scientific research and policy making.

7 Summary

385 Here, we presented a global resolved surface carbon flux dataset during the 2015–2022 period. The dataset includes 3-hourly gridded (2° latitude \times 2.5° longitude) NEE and ocean carbon fluxes (prior and posterior), together with prescribed fossil fuel emissions and biomass burning emissions. The dataset was generated by the GONGGA inversion system constrained by OCO-2 XCO₂ retrievals. We analyzed the key characteristics of the global and regional carbon cycles in terms of carbon budget, interannual variability, and seasonal cycle. The global annual estimate from GONGGA was consistent with the 390 estimate from GCB2022. Regional fluxes were analyzed based on TransCom partitions. The strongest carbon sinks were observed in Europe, followed by Boreal Asia and Temperate Asia. We validated posterior fluxes by comparing posterior simulated CO₂ concentrations with TCCON XCO₂ retrievals, as well as ObsPack surface flask and aircraft observations. Both evaluations demonstrated the optimization of posterior fluxes through assimilation of OCO-2 satellite retrievals. In the process of comparison and evaluation, we note that the observation distribution, prior estimate, and transport modeling can 395 have significant effects on inversion results; thus, they require continuous improvement by the research community.



Author contributions. TX conceptualized, administrated, and supervised the research, and acquired funds for it. JZ and WY made investigations, developed the inversion system, and visualized the data. JZ created the dataset. JZ, ZH and ZM made formal analysis of it. TX and ZH developed the methodology. TX and PS provided necessary resources. JZ wrote the original manuscript draft. TX, WY, WT, DJ and PS reviewed and edited the manuscript draft.

400 **Competing interest.** The authors declare that they have no conflict of interest.

405 **Acknowledgements.** The OCO-2 data are provided by the ACOS/OCO-2 project at the Jet Propulsion Laboratory, California Institute of Technology, and can be obtained from the data archive at the NASA Goddard Earth Science Data and Information Services Center. We acknowledge all atmospheric data providers for obspack_co2_1_GLOBALVIEWplus_v8.0_2022-08-27. We acknowledge all atmospheric data providers of TCCON GGG 2020 version.

Financial support. This work was supported by the Second Tibetan Plateau Scientific Expedition and Research Program (2022QZKK0101) and the National Natural Science Foundation of China (Grant Nos. 41975140).



410 Reference

- Ahlström, A., Raupach, M. R., Schurgers, G., Smith, B., Arneth, A., Jung, M., Reichstein, M., Canadell, J. G., Friedlingstein, P., Jain, A. K., Kato, E., Poulter, B., Sitch, S., Stocker, B. D., Viovy, N., Wang, Y. P., Wiltshire, A., Zaehle, S., and Zeng, N.: The dominant role of semi-arid ecosystems in the trend and variability of the land CO₂ sink, *Science*, 348, 895-899, <https://doi.org/10.1126/science.aaa1668>, 2015.
- 415 Andela, N. and van der Werf, G. R.: Recent trends in African fires driven by cropland expansion and El Niño to La Niña transition, *Nat. Clim. Change*, 4, 791-795, <https://doi.org/10.1038/nclimate2313>, 2014.
- Aragão, L. E. O. C., Anderson, L. O., Fonseca, M. G., Rosan, T. M., Vedovato, L. B., Wagner, F. H., Silva, C. V. J., Silva Junior, C. H. L., Arai, E., Aguiar, A. P., Barlow, J., Berenguer, E., Deeter, M. N., Domingues, L. G., Gatti, L., Gloor, M., Malhi, Y., Marengo, J. A., Miller, J. B., Phillips, O. L., and Saatchi, S.: 21st Century drought-related fires counteract the decline of Amazon deforestation carbon emissions, *Nat. Commun.*, 9, 536, <https://doi.org/10.1038/s41467-017-02771-y>, 2018.
- 420 Bacastow, R. B.: Modulation of atmospheric carbon dioxide by the Southern Oscillation, *Nature*, 261, 116-118, <https://doi.org/10.1038/261116a0>, 1976.
- Baker, D. F., Law, R. M., Gurney, K. R., Rayner, P., Peylin, P., Denning, A. S., Bousquet, P., Bruhwiler, L., Chen, Y. H., Ciais, P., Fung, I. Y., Heimann, M., John, J., Maki, T., Maksyutov, S., Masarie, K., Prather, M., Pak, B., Taguchi, S., and Zhu, Z.: TransCom 3 inversion intercomparison: Impact of transport model errors on the interannual variability of regional CO₂ fluxes, 1988–2003, *Global Biogeochem. Cy.*, 20, <https://doi.org/10.1029/2004GB002439>, 2006.
- 425 Basu, S., Guerlet, S., Butz, A., Houweling, S., Hasekamp, O., Aben, I., Krummel, P., Steele, P., Langenfelds, R., Torn, M., Biraud, S., Stephens, B., Andrews, A., and Worthy, D.: Global CO₂ fluxes estimated from GOSAT retrievals of total column CO₂, *Atmos. Chem. Phys.*, 13, 8695-8717, <https://doi.org/10.5194/acp-13-8695-2013>, 2013.
- 430 Bousquet, P., Peylin, P., Ciais, P., Le Quéré, C., Friedlingstein, P., and Tans, P. P.: Regional Changes in Carbon Dioxide Fluxes of Land and Oceans Since 1980, *Science*, 290, 1342-1346, <https://doi.org/10.1126/science.290.5495.1342>, 2000.
- Bowman, D. M. J. S., Williamson, G. J., Abatzoglou, J. T., Kolden, C. A., Cochrane, M. A., and Smith, A. M. S.: Human exposure and sensitivity to globally extreme wildfire events, *Nat. Ecol. Evol.*, 1, 0058, <https://doi.org/10.1038/s41559-016-0058>, 2017.
- 435 Braswell, B. H., Schimel, D. S., Linder, E., and Moore, B.: The response of global terrestrial ecosystems to interannual temperature variability, *Science*, 278, 870-872, <https://doi.org/10.1126/science.278.5339.870>, 1997.
- Buschmann, M., Petri, C., Palm, M., Warncke, T., and Notholt, J.: TCCON data from Ny-Ålesund, Svalbard (NO), Release GGG2020.R0 (R0) [dataset], <https://doi.org/10.14291/tccon.ggg2020.nyalesund01.R0>, 2022.
- Byrne, B., Jones, D. B. A., Strong, K., Zeng, Z. C., Deng, F., and Liu, J.: Sensitivity of CO₂ surface flux constraints to observational coverage, *J. Geophys. Res.-Atmos.*, 122, 6672-6694, <https://doi.org/10.1002/2016jd026164>, 2017.
- 440 Chen, J. M.: Carbon neutrality: Toward a sustainable future, *The Innovation*, 2, 100127, <https://doi.org/10.1016/j.xinn.2021.100127>, 2021.
- Chevallier, F., Palmer, P. I., Feng, L., Boesch, H., O'Dell, C. W., and Bousquet, P.: Toward robust and consistent regional CO₂ flux estimates from in situ and spaceborne measurements of atmospheric CO₂, *Geophys. Res. Lett.*, 41, 1065-1070, <https://doi.org/10.1002/2013gl058772>, 2014.
- 445 Chevallier, F., Remaud, M., O'Dell, C. W., Baker, D., Peylin, P., and Cozic, A.: Objective evaluation of surface- and satellite-driven carbon dioxide atmospheric inversions, *Atmos. Chem. Phys.*, 19, 14233-14251, <https://doi.org/10.5194/acp-19-14233-2019>, 2019.
- Chevallier, F., Ciais, P., Conway, T. J., Aalto, T., Anderson, B. E., Bousquet, P., Brunke, E. G., Ciattaglia, L., Esaki, Y., Froehlich, M., Gomez, A., Gomez-Pelaez, A. J., Haszpra, L., Krummel, P. B., Langenfelds, R. L., Leuenberger, M., Machida, T., Maignan, F., Matsueda, H., Morgui, J. A., Mukai, H., Nakazawa, T., Peylin, P., Ramonet, M., Rivier, L., Sawa, Y., Schmidt, M., Steele, L. P., Vay, S. A., Vermeulen, A. T., Wofsy, S., and Worthy, D.: CO₂ surface fluxes at grid point scale estimated from a global 21 year reanalysis of atmospheric measurements, *J. Geophys. Res.-Atmos.*, 115, D21307, <https://doi.org/10.1029/2010jd013887>, 2010.
- Connor, B. J., Boesch, H., Toon, G., Sen, B., Miller, C., and Crisp, D.: Orbiting carbon observatory: Inverse method and prospective error analysis, *J. Geophys. Res.-Atmos.*, 113, D05305, <https://doi.org/10.1029/2006jd008336>, 2008.
- 450 Cox, A., Di Sarra, A. G., Vermeulen, A., Manning, A., Beyersdorf, A., Zahn, A., Manning, A., Watson, A., Karion, A., Hoheisel, A., Leskinen, A., Hensen, A., Arlyn, A., Jordan, A., Frumau, A., Colomb, A., Scheeren, B., Law, B., Baier, B., Munger, B., Paplawsky, B., Viner, B., Stephens, B., Daube, B., Labuschagne, C., Myhre, C. L., Couret, C., Hanson, C., Miller, C. E., Lunder, C. R., Plass-Duelmer, C., Plass-Duelmer, C., Gerbig, C., Sloop, C. D., Sweeney, C., Kubistin, D., Goto, D., Jaffe, D., Heltai, D., Van Dinther, D., Bowling, D., Lam, D. H. Y., Munro, D., Dickon, Y., Worthy, D., Dlugokencky, E., Kozlova, E., Gloor, E., Cuevas, E., Reyes-Sanchez, E., Hints, E., Kort, E., Morgan, E., Obersteiner, F., Apadula, F., Francois, G., Meinhardt, F., Moore, F., Vitkova, G., Chen, G., Bentz, G., Giordane, A. M., Manca, G., Brailsford, G., Forster, G., Boenisch, H., Riris, H., Meijer, H., Moossern, H., Timas, H., Matsueda, H., Huilin, C., Levin, I., Lehner, I., Mammarella, I., Bartyzel, J., Abshire, J. B., Elkins, J. W., Levula, J., Jaroslaw, N., Pichon, J. M., Peischl, J., Müller-Williams, J., Turnbull, J., Miller, J. B., Lee, J., Lin, J., Jooil, K., Josep-Anton, M., Pitt, J., DiGangi, J. P., Lavric, J., Hatakka, J., Coletta, J. D., Worsey, J., Holst, J., Lehtinen, K., Kominkova, K., McKain, K., Saito, K., Aikin, K., Davis, K., Thoning, K., Tørseth, K., Haszpra, L., Sørensen, L. L., Mitchell, L., Gatti, L. V., Emmenegger, L., Lukasz, C., Merchant, L., Sha, M. K., Delmotte, M., Fischer, M. L., Schumacher, M., Torn, M., Leuenberger, M., Heimann, M., Heimann,



- 465 M., Steinbacher, M., Schmidt, M., De Mazière, M., Sargent, M., Lindauer, M., Mölder, M., Martin, M. Y., Rothe, M., Shook, M., Galkowski, M., Heliasz, M., Marek, M. V., Ramonet, M., Miroslaw, Z., Lopez, M., Sasakawa, M., Mihalopoulos, N., Miles, N., Lee, O. S. M., Laurent, O., Peltola, O., Hermanssen, O., Trisolino, P., Cristofanelli, P., Kolari, P., Krummel, P., Shepson, P., Smith, P., Rivas, P. P., Bakwin, P., Bergamaschi, P., Keronen, P., Tans, P., Van Den Bulk, P., Keeling, R., Ramos, R., Langenfelds, R., Weiss, R., Leppert, R., De Souza, R. A. F., Curcoll, R., Commane, R., Newman, S., Piacentino, S., Hammer, S., Richardson, S., Biraud, S. C., Conil, S., Clark, S., Morimoto, S., Shuangxi, F., Aoki, S., O'Doherty, S., Sites, C., Zaehle, S., De Wekker, S., Kawa, S. R., Platt, S. M., Montzka, S., Walker, S., Piper, S., Prinzivalli, S., Wofsy, S., Nichol, S., Schuck, T., Lauvaux, T., Ryerson, T., Seifert, T., Griffis, T., Biermann, T., Kneuer, T., Gehrelein, T., Machida, T., Laurila, T., Aalto, T., Gomez-Trueba, V., Kazan, V., Ivakhov, V., Joubert, W., Brand, W. A., Lan, X., Niwa, Y., and Loh, Z.: Multi-laboratory compilation of atmospheric carbon dioxide data for the period 1957-2021; obspack_co2_1_GLOBALVIEWplus_v8.0_2022-08-27, NOAA Global Monitoring Laboratory [dataset], <https://doi.org/10.25925/20220808>, 2022.
- 470 Crisp, D., Atlas, R. M., Breon, F. M., Brown, L. R., Burrows, J. P., Ciais, P., Connor, B. J., Doney, S. C., Fung, I. Y., Jacob, D. J., Miller, C. E., O'Brien, D., Pawson, S., Randerson, J. T., Rayner, P., Salawitch, R. J., Sander, S. P., Sen, B., Stephens, G. L., Tans, P. P., Toon, G. C., Wennberg, P. O., Wofsy, S. C., Yung, Y. L., Kuang, Z. M., Chudasama, B., Sprague, G., Weiss, B., Pollock, R., Kenyon, D., and Schroll, S.: The orbiting carbon observatory (OCO) mission, *Adv. Space Res.*, 34, 700-709, <https://doi.org/10.1016/j.asr.2003.08.062>, 2004.
- 475 Crisp, D., Fisher, B. M., O'Dell, C., Frankenberg, C., Basilio, R., Bösch, H., Brown, L. R., Castano, R., Connor, B., Deutscher, N. M., Eldering, A., Griffith, D., Gunson, M., Kuze, A., Mandrake, L., McDuffie, J., Messerschmidt, J., Miller, C. E., Morino, I., Natraj, V., Notholt, J., O'Brien, D. M., Oyafuso, F., Polonsky, I., Robinson, J., Salawitch, R., Sherlock, V., Smyth, M., Suto, H., Taylor, T. E., Thompson, D. R., Wennberg, P. O., Wunch, D., and Yung, Y. L.: The ACOS CO₂ retrieval algorithm - Part 2: Global XCO₂ data characterization, *Atmos. Meas. Tech.*, 5, 687-707, <https://doi.org/10.5194/amt-5-687-2012>, 2012.
- 480 Crowell, S., Baker, D., Schuh, A., Basu, S., Jacobson, A. R., Chevallier, F., Liu, J., Deng, F., Feng, L., McKain, K., Chatterjee, A., Miller, J. B., Stephens, B. B., Eldering, A., Crisp, D., Schimel, D., Nassar, R., O'Dell, C., Oda, T., Sweeney, C., Palmer, P. I., and Jones, D. B. A.: The 2015-2016 carbon cycle as seen from OCO-2 and the global in situ network, *Atmos. Chem. Phys.*, 19, 9797-9831, <https://doi.org/10.5194/acp-19-9797-2019>, 2019.
- 485 Dannenberg, M. P., Smith, W. K., Zhang, Y., Song, C., Huntzinger, D. N., and Moore, D. J. P.: Large-scale reductions in terrestrial carbon uptake following central pacific El Niño, *Geophys. Res. Lett.*, 48, e2020GL092367, <https://doi.org/10.1029/2020gl092367>, 2021.
- 490 De Mazière, M., Sha, M. K., Desmet, F., Hermans, C., Scolas, F., Kumps, N., Zhou, M., Metzger, J.-M., Duflot, V., and Cammas, J.-P.: TCCON data from Réunion Island (RE), Release GGG2020.R0 (R0) [dataset], <https://doi.org/10.14291/tcon.ggg2020.reunion01.R0>, 2022.
- 495 Deutscher, N. M., Griffith, D. W. T., Paton-Walsh, C., Jones, N. B., Velasco, V. A., Wilson, S. R., Macatangay, R. C., Kettlewell, G. C., Buchholz, R. R., Riggenbach, M. O., Bukosa, B., John, S. S., Walker, B. T., and Nawaz, H.: TCCON data from Wollongong (AU), Release GGG2020.R0 (R0) [dataset], <https://doi.org/10.14291/tcon.ggg2020.wollongong01.R0>, 2023.
- 500 Dubey, M. K., Henderson, B. G., Allen, N. T., Blavier, J.-F., Roehl, C. M., and Wunch, D.: TCCON data from Manaus (BR), Release GGG2020.R0 (R0) [dataset], <https://doi.org/10.14291/tcon.ggg2020.manaus01.R0>, 2022.
- 505 Elderling, A., Wennberg, P. O., Crisp, D., Schimel, D. S., Gunson, M. R., Chatterjee, A., Liu, J., Schwandner, F. M., Sun, Y., O'Dell, C. W., Frankenberg, C., Taylor, T., Fisher, B., Osterman, G. B., Wunch, D., Hakkarainen, J., Tamminen, J., and Weir, B.: The Orbiting Carbon Observatory-2 early science investigations of regional carbon dioxide fluxes, *Science*, 358, eaam5745, <https://doi.org/10.1126/science.aam5745>, 2017.
- 510 Forkel, M., Carvalhais, N., Rödenbeck, C., Keeling, R., Heimann, M., Thonicke, K., Zaehle, S., and Reichstein, M.: Enhanced seasonal CO₂ exchange caused by amplified plant productivity in northern ecosystems, *Science*, 351, 696-699, <https://doi.org/10.1126/science.aac4971>, 2016.
- 515 Friedlingstein, P., O'Sullivan, M., Jones, M. W., Andrew, R. M., Gregor, L., Hauck, J., Le Quéré, C., Luijkh, I. T., Olsen, A., Peters, G. P., Peters, W., Pongratz, J., Schwingsackl, C., Sitch, S., Canadell, J. G., Ciais, P., Jackson, R. B., Alin, S. R., Alkama, R., Arneth, A., Arora, V. K., Bates, N. R., Becker, M., Bellouin, N., Bittig, H. C., Bopp, L., Chevallier, F., Chini, L. P., Cronin, M., Evans, W., Falk, S., Feely, R. A., Gasser, T., Gehlen, M., Grätz, T., Gloege, L., Grassi, G., Gruber, N., Gürses, Ö., Harris, I., Hefner, M., Houghton, R. A., Hurtt, G. C., Iida, Y., Ilyina, T., Jain, A. K., Jersild, A., Kadono, K., Kato, E., Kennedy, D., Klein Goldewijk, K., Knauer, J., Korsbakken, J. I., Landschützer, P., Lefèvre, N., Lindsay, K., Liu, J., Liu, Z., Marland, G., Mayot, N., McGrath, M. J., Metzl, N., Monacci, N. M., Munro, D. R., Nakao, S. I., Niwa, Y., O'Brien, K., Ono, T., Palmer, P. I., Pan, N., Pierrot, D., Pocock, K., Poulet, B., Resplandy, L., Robertson, E., Rödenbeck, C., Rodriguez, C., Rosan, T. M., Schwinger, J., Séférian, R., Shutler, J. D., Skjelvan, I., Steinhoff, T., Sun, Q., Sutton, A. J., Sweeney, C., Takao, S., Tanhua, T., Tans, P. P., Tian, X., Tian, H., Tilbrook, B., Tsujino, H., Tubiello, F., van der Werf, G. R., Walker, A. P., Wanninkhof, R., Whitehead, C., Willstrand Wranne, A., Wright, R., Yuan, W., Yue, C., Yue, X., Zaehle, S., Zeng, J., and Zheng, B.: Global Carbon Budget 2022, *Earth Syst. Sci. Data*, 14, 4811-4900, <https://doi.org/10.5194/essd-14-4811-2022>, 2022.
- 520 García, O. E., Schneider, M., Herkommer, B., Gross, J., Hase, F., Blumenstock, T., and Sepúlveda, E.: TCCON data from Izana (ES), Release GGG2020.R1 (R1) [dataset], <https://doi.org/10.14291/tcon.ggg2020.izana01.R1>, 2022.



- Gelaro, R., McCarty, W., Suárez, M. J., Todling, R., Molod, A., Takacs, L., Randles, C. A., Darmenov, A., Bosilovich, M. G., Reichle, R., Wargan, K., Coy, L., Cullather, R., Draper, C., Akella, S., Buchard, V., Conaty, A., da Silva, A. M., Gu, W., Kim, G.-K., Koster, R., Lucchesi, R., Merkova, D., Nielsen, J. E., Partyka, G., Pawson, S., Putman, W., Rienecker, M., Schubert, S. D., Sienkiewicz, M., and Zhao, B.: The modern-era retrospective analysis for research and applications, version 2 (MERRA-2), *J. Climate*, 30, 5419–5454, <https://doi.org/10.1175/JCLI-D-16-0758.1>, 2017.
- 525 Giglio, L., Randerson, J. T., and van der Werf, G. R.: Analysis of daily, monthly, and annual burned area using the fourth-generation global fire emissions database (GFED4), *J. Geophys. Res.-Biogeosci.*, 118, 317–328, <https://doi.org/10.1002/jgrg.20042>, 2013.
- Graven, H. D., Keeling, R. F., Piper, S. C., Patra, P. K., Stephens, B. B., Wofsy, S. C., Welp, L. R., Sweeney, C., Tans, P. P., Kelley, J. J., Daube, B. C., Kort, E. A., Santoni, G. W., and Bent, J. D.: Enhanced Seasonal Exchange of CO₂ by Northern Ecosystems Since 530 1960, *Science*, 341, 1085–1089, <https://doi.org/10.1126/science.1239207>, 2013.
- Gu, G. and Adler, R. F.: Precipitation and Temperature Variations on the Interannual Time Scale: Assessing the Impact of ENSO and Volcanic Eruptions, *J. Climate*, 24, 2258–2270, <https://doi.org/10.1175/2010JCLI3727.1>, 2011.
- 535 Guimbberteau, M., Zhu, D., Maignan, F., Huang, Y., Yue, C., Dantec-Nédélec, S., Ottlé, C., Jornet-Puig, A., Bastos, A., Laurent, P., Goll, D., Bowring, S., Chang, J., Guenet, B., Tifafi, M., Peng, S., Krinner, G., Ducharne, A., Wang, F., Wang, T., Wang, X., Wang, Y., Yin, Z., Lauwald, R., Joetzjer, E., Qiu, C., Kim, H., and Ciais, P.: ORCHIDEE-MICT (v8.4.1), a land surface model for the high latitudes: model description and validation, *Geosci. Model Dev.*, 11, 121–163, 10.5194/gmd-11-121-2018, 2018.
- Gunson, M. and Eldering, A.: OCO-2 Level 2 bias-corrected XCO₂ and other select fields from the full-physics retrieval aggregated as 540 daily files, Retrospective processing V10r, Greenbelt, MD, USA, Goddard Earth Sciences Data and Information Services Center (GES DISC) [dataset], <https://doi.org/10.5067/E4E140XDMPO2>, 2020.
- Gurney, K. R., Law, R. M., Denning, A. S., Rayner, P. J., Pak, B. C., Baker, D., Bousquet, P., Bruhwiler, L., Chen, Y. H., Ciais, P., Fung, I. Y., Heimann, M., John, J., Maki, T., Maksyutov, S., Peylin, P., Prather, M., and Taguchi, S.: Transcom 3 inversion intercomparison: Model mean results for the estimation of seasonal carbon sources and sinks, *Global Biogeochem. Cy.*, 18, <https://doi.org/10.1029/2003GB002111>, 2004.
- 545 Gurney, K. R., Law, R. M., Denning, A. S., Rayner, P. J., Baker, D., Bousquet, P., Bruhwiler, L., Chen, Y.-H., Ciais, P., Fan, S., Fung, I. Y., Gloo, M., Heimann, M., Higuchi, K., John, J., Maki, T., Maksyutov, S., Masarie, K., Peylin, P., Prather, M., Pak, B. C., Randerson, J., Sarmiento, J., Taguchi, S., Takahashi, T., and Yuen, C.-W.: Towards robust regional estimates of CO₂ sources and sinks using atmospheric transport models, *Nature*, 415, 626–630, <https://doi.org/10.1038/415626a>, 2002.
- Hase, F., Herkommmer, B., Groß, J., Blumenstock, T., Kiel, M. ä., and Dohe, S.: TCCON data from Karlsruhe (DE), Release GGG2020.R0 (R0) [dataset], <https://doi.org/10.14291/tccon.ggg2020.karlsruhe01.R0>, 2022.
- 550 Hauck, J., Zeising, M., Le Quere, C., Gruber, N., Bakker, D. C. E., Bopp, L., Chau, T. T. T., Guerres, O., Ilyina, T., Landschuetzer, P., Lenton, A., Resplandy, L., Roedenbeck, C., Schwinger, J., and Seferian, R.: Consistency and challenges in the ocean carbon sink estimate for the global carbon budget, *Front. Mar. Sci.*, 7, 571720, <https://doi.org/10.3389/fmars.2020.571720>, 2020.
- Iraci, L. T., Podolske, J. R., Roehl, C., Wennberg, P. O., Blavier, J.-F., Allen, N., Wunch, D., and Osterman, G. B.: TCCON data from Edwards (US), Release GGG2020.R0 (R0) [dataset], <https://doi.org/10.14291/tccon.ggg2020.edwards01.R0>, 2022.
- 555 Jiang, F., Ju, W., He, W., Wu, M., Wang, H., Wang, J., Jia, M., Feng, S., Zhang, L., and Chen, J. M.: A 10-year global monthly averaged terrestrial net ecosystem exchange dataset inferred from the ACOS GOSAT v9 XCO₂ retrievals (GCAS2021), *Earth Syst. Sci. Data*, 14, 3013–3037, <https://doi.org/10.5194/essd-14-3013-2022>, 2022.
- Jin, Z., Tian, X., Wang, Y., Wang, T., and Piao, S.: A global surface CO₂ flux dataset (2015–2022) inferred from OCO-2 retrievals using the GONGGA inversion system [dataset], <https://doi.org/10.5281/zenodo.8368846>, 2023a.
- 560 Jin, Z., Wang, T., Zhang, H., Wang, Y., Ding, J., and Tian, X.: Constraint of satellite CO₂ retrieval on the global carbon cycle from a Chinese atmospheric inversion system, *Sci. China Earth Sci.*, 66, <https://doi.org/10.1007/s11430-022-1036-7>, 2023b.
- Jones, C. D., Collins, M., Cox, P. M., and Spall, S. A.: The Carbon Cycle Response to ENSO: A Coupled Climate–Carbon Cycle Model Study, *J. Climate*, 14, 4113–4129, [https://doi.org/10.1175/1520-0442\(2001\)014<4113:TCCRTE>2.0.CO;2](https://doi.org/10.1175/1520-0442(2001)014<4113:TCCRTE>2.0.CO;2), 2001.
- Jones, M. W., Andrew, R. M., Peters, G. P., Janssens-Maenhout, G., De-Gol, A. J., Ciais, P., Patra, P. K., Chevallier, F., and Le Quere, C.: 565 Gridded fossil CO₂ emissions and related O₂ combustion consistent with national inventories 1959–2018, *Sci. Data*, 8, 2, <https://doi.org/10.1038/s41597-020-00779-6>, 2021.
- Jung, M., Schwalm, C., Migliavacca, M., Walther, S., Camps-Valls, G., Koitala, S., Anthoni, P., Besnard, S., Bodesheim, P., Carvalhais, N., Chevallier, F., Gans, F., Goll, D. S., Haverd, V., Köhler, P., Ichii, K., Jain, A. K., Liu, J., Lombardozzi, D., Nabel, J. E. M. S., Nelson, J. A., O'Sullivan, M., Pallandt, M., Papale, D., Peters, W., Pongratz, J., Rödenbeck, C., Sitch, S., Tramontana, G., Walker, A., Weber, U., and Reichstein, M.: Scaling carbon fluxes from eddy covariance sites to globe: synthesis and evaluation of the FLUXCOM approach, *Biogeosciences*, 17, 1343–1365, <https://doi.org/10.5194/bg-17-1343-2020>, 2020.
- Kiel, M., O'Dell, C. W., Fisher, B., Eldering, A., Nassar, R., MacDonald, C. G., and Wennberg, P. O.: How bias correction goes wrong: Measurement of XCO₂ affected by erroneous surface pressure estimates, *Atmos. Meas. Tech.*, 12, 2241–2259, <https://doi.org/10.5194/amt-12-2241-2019>, 2019.
- 570 575 Kivi, R., Heikkinen, P., and Kyrö, E.: TCCON data from Sodankylä (FI), Release GGG2020.R0 (R0) [dataset], <https://doi.org/10.14291/tccon.ggg2020.sodankyla01.R0>, 2022.



- Lauvaux, T., Miles, N. L., Deng, A., Richardson, S. J., Cambaliza, M. O., Davis, K. J., Gaudet, B., Gurney, K. R., Huang, J., O'Keefe, D., Song, Y., Karion, A., Oda, T., Patarasuk, R., Razlivanova, I., Sarmiento, D., Shepson, P., Sweeney, C., Turnbull, J., and Wu, K.: High-resolution atmospheric inversion of urban CO₂ emissions during the dormant season of the Indianapolis Flux Experiment (INFLUX), *J. Geophys. Res.-Atmos.*, 121, 5213-5236, <https://doi.org/10.1002/2015jd024473>, 2016.
- 580 Lin, X., Rogers, B. M., Sweeney, C., Chevallier, F., Arshinov, M., Dlugokencky, E., Machida, T., Sasakawa, M., Tans, P., and Keppel-Aleks, G.: Siberian and temperate ecosystems shape Northern Hemisphere atmospheric CO₂ seasonal amplification, *P. Natl. Acad. Sci. USA*, 117, 21079-21087, <https://doi.org/10.1073/pnas.1914135117>, 2020.
- 585 Liu, C., Wang, W., Sun, Y., and Shan, C.: TCCON data from Hefei (PRC), Release GGG2020.R0 (R0) [dataset], <https://doi.org/10.14291/tccon.ggg2020.hefei01.R0>, 2022.
- Liu, J., Bowman, K. W., Schimel, D. S., Parazoo, N. C., Jiang, Z., Lee, M., Bloom, A. A., Wunch, D., Frankenberg, C., Sun, Y., O'Dell, C. W., Gurney, K. R., Menemenlis, D., Gierach, M., Crisp, D., and Eldering, A.: Contrasting carbon cycle responses of the tropical continents to the 2015-2016 El Niño, *Science*, 358, eaam5690, <https://doi.org/10.1126/science.aam5690>, 2017.
- 590 Liu, J., Baskaran, L., Bowman, K., Schimel, D., Bloom, A. A., Parazoo, N. C., Oda, T., Carroll, D., Menemenlis, D., Joiner, J., Commane, R., Daube, B., Gatti, L. V., McKain, K., Miller, J., Stephens, B. B., Sweeney, C., and Wofsy, S.: Carbon monitoring system flux net biosphere exchange 2020 (CMS-Flux NBE 2020), *Earth Syst. Sci. Data*, 13, 299-330, <https://doi.org/10.5194/essd-13-299-2021>, 2021.
- Masarie, K. A., Peters, W., Jacobson, A. R., and Tans, P. P.: ObsPack: a framework for the preparation, delivery, and attribution of atmospheric greenhouse gas measurements, *Earth Syst. Sci. Data*, 6, 375-384, <https://doi.org/10.5194/essd-6-375-2014>, 2014.
- 595 Miller, S. M. and Michalak, A. M.: The impact of improved satellite retrievals on estimates of biospheric carbon balance, *Atmos. Chem. Phys.*, 20, 323-331, <https://doi.org/10.5194/acp-20-323-2020>, 2020.
- Miller, S. M., Michalak, A. M., Yadav, V., and Tadic, J. M.: Characterizing biospheric carbon balance using CO₂ observations from the OCO-2 satellite, *Atmos. Chem. Phys.*, 18, 6785-6799, <https://doi.org/10.5194/acp-18-6785-2018>, 2018.
- 600 Morino, I., Ohyama, H., Hori, A., and Ikegami, H.: TCCON data from Tsukuba (JP), 125HR, Release GGG2020.R0 (R0) [dataset], <https://doi.org/10.14291/tccon.ggg2020.tsukuba02.R0>, 2022a.
- Morino, I., Ohyama, H., Hori, A., and Ikegami, H.: TCCON data from Rikubetsu (JP), Release GGG2020.R0 (R0) [dataset], <https://doi.org/10.14291/tccon.ggg2020.rikubetsu01.R0>, 2022b.
- 605 Morino, I., Velazco, V. A., Hori, A., Uchino, O., and Griffith, D. W. T.: TCCON data from Burgos, Ilocos Norte (PH), Release GGG2020.R0 (R0) [dataset], <https://doi.org/10.14291/tccon.ggg2020.burgos01.R0>, 2022c.
- Moritz, M. A., Batllori, E., Bradstock, R. A., Gill, A. M., Handmer, J., Hessburg, P. F., Leonard, J., McCaffrey, S., Odion, D. C., Schoennagel, T., and Syphard, A. D.: Learning to coexist with wildfire, *Nature*, 515, 58-66, <https://doi.org/10.1038/nature13946>, 2014.
- 610 Nassar, R., Napier-Linton, L., Gurney, K. R., Andres, R. J., Oda, T., Vogel, F. R., and Deng, F.: Improving the temporal and spatial distribution of CO₂ emissions from global fossil fuel emission data sets, *J. Geophys. Res.-Atmos.*, 118, 917-933, <https://doi.org/10.1029/2012jd018196>, 2013.
- Nassar, R., Jones, D. B. A., Kulawik, S. S., Worden, J. R., Bowman, K. W., Andres, R. J., Suntharalingam, P., Chen, J. M., Brenninkmeijer, C. A. M., Schuck, T. J., Conway, T. J., and Worthy, D. E.: Inverse modeling of CO₂ sources and sinks using satellite observations of CO₂ from TES and surface flask measurements, *Atmos. Chem. Phys.*, 11, 6029-6047, <https://doi.org/10.5194/acp-11-6029-2011>, 2011.
- 615 Nassar, R., Jones, D. B. A., Suntharalingam, P., Chen, J. M., Andres, R. J., Wecht, K. J., Yantosca, R. M., Kulawik, S. S., Bowman, K. W., Worden, J. R., Machida, T., and Matsueda, H.: Modeling global atmospheric CO₂ with improved emission inventories and CO₂ production from the oxidation of other carbon species, *Geosci. Model Dev.*, 3, 689-716, <https://doi.org/10.5194/gmd-3-689-2010>, 2010.
- Notholt, J., Petri, C., Warneke, T., and Buschmann, M.: TCCON data from Bremen (DE), Release GGG2020.R0 (R0) [dataset], <https://doi.org/10.14291/tccon.ggg2020.bremen01.R0>, 2022.
- 620 O'Dell, C. W., Connor, B., Bösch, H., O'Brien, D., Frankenberg, C., Castano, R., Christi, M., Eldering, D., Fisher, B., Gunson, M., McDuffie, J., Miller, C. E., Natraj, V., Oyafuso, F., Polonsky, I., Smyth, M., Taylor, T., Toon, G. C., Wennberg, P. O., and Wunch, D.: The ACOS CO₂ retrieval algorithm – part 1: description and validation against synthetic observations, *Atmos. Meas. Tech.*, 5, 99-121, <https://doi.org/10.5194/amt-5-99-2012>, 2012.
- 625 O'Dell, C. W., Eldering, A., Wennberg, P. O., Crisp, D., Gunson, M. R., Fisher, B., Frankenberg, C., Kiel, M., Lindqvist, H., Mandrake, L., Merrelli, A., Natraj, V., Nelson, R. R., Osterman, G. B., Payne, V. H., Taylor, T. E., Wunch, D., Drouin, B. J., Oyafuso, F., Chang, A., McDuffie, J., Smyth, M., Baker, D. F., Basu, S., Chevallier, F., Crowell, S. M. R., Feng, L., Palmer, P. I., Dubey, M., García, O. E., Griffith, D. W. T., Hase, F., Iraci, L. T., Kivi, R., Morino, I., Notholt, J., Ohyama, H., Petri, C., Roehl, C. M., Sha, M. K., Strong, K., Sussmann, R., Te, Y., Uchino, O., and Velazco, V. A.: Improved retrievals of carbon dioxide from Orbiting Carbon Observatory-2 with the version 8 ACOS algorithm, *Atmos. Meas. Tech.*, 11, 6539-6576, <https://doi.org/10.5194/amt-11-6539-2018>, 2018.
- 630



- Peiro, H., Crowell, S., Schuh, A., Baker, D. F., O'Dell, C., Jacobson, A. R., Chevallier, F., Liu, J., Eldering, A., Crisp, D., Deng, F., Weir, B., Basu, S., Johnson, M. S., Philip, S., and Baker, I.: Four years of global carbon cycle observed from the Orbiting Carbon Observatory 2 (OCO-2) version 9 and in situ data and comparison to OCO-2 version 7, *Atmos. Chem. Phys.*, 22, 1097-1130, <https://doi.org/10.5194/acp-22-1097-2022>, 2022.
- Peters, W., Jacobson, A. R., Sweeney, C., Andrews, A. E., Conway, T. J., Masarie, K., Miller, J. B., Bruhwiler, L. M. P., Petron, G., Hirsch, A. I., Worthy, D. E. J., van der Werf, G. R., Randerson, J. T., Wennberg, P. O., Krol, M. C., and Tans, P. P.: An atmospheric perspective on North American carbon dioxide exchange: CarbonTracker, *P. Natl. Acad. Sci. USA*, 104, 18925-18930, <https://doi.org/10.1073/pnas.0708986104>, 2007.
- Petri, C., Vrekoussis, M., Rousogenous, C., Warneke, T., Sciare, J., and Notholt, J.: TCCON data from Nicosia, Cyprus (CY), Release GGG2020.R0 (R0) [dataset], <https://doi.org/10.14291/tcon.ggg2020.nicosia01.R0>, 2022.
- Peylin, P., Law, R. M., Gurney, K. R., Chevallier, F., Jacobson, A. R., Maki, T., Niwa, Y., Patra, P. K., Peters, W., Rayner, P. J., Roedenbeck, C., van der Laan-Luijkx, I. T., and Zhang, X.: Global atmospheric carbon budget: results from an ensemble of atmospheric CO₂ inversions, *Biogeosciences*, 10, 6699-6720, <https://doi.org/10.5194/bg-10-6699-2013>, 2013.
- Piao, S., He, Y., Wang, X., and Chen, F.: Estimation of China's terrestrial ecosystem carbon sink: methods, progress and prospects, *Sci. China Earth Sci.*, 65, 641-651, <https://doi.org/10.1007/s11430-021-9892-6>, 2022.
- Piao, S., Ciais, P., Friedlingstein, P., de Noblet-Ducoudré, N., Cadule, P., Viovy, N., and Wang, T.: Spatiotemporal patterns of terrestrial carbon cycle during the 20th century, *Global Biogeochem. Cy.*, 23, GB4026, <https://doi.org/10.1029/2008gb003339>, 2009a.
- Piao, S., Fang, J., Ciais, P., Peylin, P., Huang, Y., Sitch, S., and Wang, T.: The carbon balance of terrestrial ecosystems in China, *Nature*, 458, 1009-U1082, <https://doi.org/10.1038/nature07944>, 2009b.
- Piao, S., Wang, X., Wang, K., Li, X., Bastos, A., Canadell, J. G., Ciais, P., Friedlingstein, P., and Sitch, S.: Interannual variation of terrestrial carbon cycle: issues and perspectives, *Glob. Change Biol.*, 26, 300-318, <https://doi.org/10.1111/gcb.14884>, 2020.
- Pollard, D. F., Robinson, J., and Shiona, H.: TCCON data from Lauder (NZ), Release GGG2020.R0 (R0) [dataset], <https://doi.org/10.14291/tcon.ggg2020.lauder03.R0>, 2022.
- Potter, C. S., Randerson, J. T., Field, C. B., Matson, P. A., Vitousek, P. M., Mooney, H. A., and Klooster, S. A.: Terrestrial ecosystem production - a process model-based on global satellite and surface data, *Global Biogeochem. Cy.*, 7, 811-841, <https://doi.org/10.1029/93gb02725>, 1993.
- Randerson, J. T., Thompson, M. V., Conway, T. J., Fung, I. Y., and Field, C. B.: The contribution of terrestrial sources and sinks to trends in the seasonal cycle of atmospheric carbon dioxide, *Global Biogeochem. Cy.*, 11, 535-560, <https://doi.org/10.1029/97GB02268>, 1997.
- Randerson, J. T., Van Der Werf, G. R., Giglio, L., Collatz, G. J., and Kasibhatla, P. S.: Global Fire Emissions Database, Version 4.1 (GFEDv4), ORNL Distributed Active Archive Center [dataset], <https://doi.org/10.3334/ORNLDaac/1293>, 2017.
- Raupach, M. R., Canadell, J. G., and Le Quere, C.: Anthropogenic and biophysical contributions to increasing atmospheric CO₂ growth rate and airborne fraction, *Biogeosciences*, 5, 1601-1613, <https://doi.org/10.5194/bg-5-1601-2008>, 2008.
- Rayner, P. J., Law, R. M., Allison, C. E., Francey, R. J., Trudinger, C. M., and Pickett-Heaps, C.: Interannual variability of the global carbon cycle (1992–2005) inferred by inversion of atmospheric CO₂ and δ¹³CO₂ measurements, *Global Biogeochem. Cy.*, 22, <https://doi.org/10.1029/2007GB003068>, 2008.
- Regnier, P., Resplandy, L., Najjar, R. G., and Ciais, P.: The land-to-ocean loops of the global carbon cycle, *Nature*, 603, 401-410, 10.1038/s41586-021-04339-9, 2022.
- Rödenbeck, C., Zaehle, S., Keeling, R., and Heimann, M.: History of El Niño impacts on the global carbon cycle 1957–2017: a quantification from atmospheric CO₂ data, *Philos. T. R. Soc. B*, 373, 20170303, <https://doi.org/10.1098/rstb.2017.0303>, 2018a.
- Rödenbeck, C., Zaehle, S., Keeling, R., and Heimann, M.: How does the terrestrial carbon exchange respond to inter-annual climatic variations? A quantification based on atmospheric CO₂ data, *Biogeosciences*, 15, 2481-2498, <https://doi.org/10.5194/bg-15-2481-2018>, 2018b.
- Schuh, A. E., Jacobson, A. R., Basu, S., Weir, B., Baker, D., Bowman, K., Chevallier, F., Crowell, S., Davis, K. J., Deng, F., Denning, S., Feng, L., Jones, D., Liu, J., and Palmer, P. I.: Quantifying the Impact of Atmospheric Transport Uncertainty on CO₂ Surface Flux Estimates, *Global Biogeochem. Cy.*, 33, 484-500, <https://doi.org/10.1029/2018GB006086>, 2019.
- Sherlock, V., Connor, B., Robinson, J., Shiona, H., Smale, D., and Pollard, D. F.: TCCON data from Lauder (NZ), 125HR, Release GGG2020.R0 (R0) [dataset], <https://doi.org/10.14291/tcon.ggg2020.lauder02.R0>, 2022.
- Shiomii, K., Kawakami, S., Ohyama, H., Arai, K., Okumura, H., Ikegami, H., and Usami, M.: TCCON data from Saga (JP), Release GGG2020.R0 (R0) [dataset], <https://doi.org/10.14291/tcon.ggg2020.saga01.R0>, 2022.
- Strong, K., Roche, S., Franklin, J. E., Mendonca, J., Lutsch, E., Weaver, D., Fogal, P. F., Drummond, J. R., Batchelor, R., Lindenmaier, R., and McGee, E.: TCCON data from Eureka (CA), Release GGG2020.R0 (R0) [dataset], <https://doi.org/10.14291/tcon.ggg2020.eureka01.R0>, 2022.
- Suntharalingam, P., Jacob, D. J., Palmer, P. I., Logan, J. A., Yantosca, R. M., Xiao, Y. P., Evans, M. J., Streets, D. G., Vay, S. L., and Sachse, G. W.: Improved quantification of Chinese carbon fluxes using CO₂/CO correlations in Asian outflow, *J. Geophys. Res.-Atmos.*, 109, D18S18, <https://doi.org/10.1029/2003jd004362>, 2004.



- Sussmann, R. and Rettinger, M.: TCCON data from Garmisch (DE), Release GGG2020.R0 (R0) [dataset], <https://doi.org/10.14291/tcon.ggg2020.garmisch01.R0>, 2022.
- 690 Takagi, H., Saeki, T., Oda, T., Saito, M., Valsala, V., Belikov, D., Saito, R., Yoshida, Y., Morino, I., Uchino, O., Andres, R. J., Yokota, T., and Maksyutov, S.: On the benefit of GOSAT observations to the estimation of regional CO₂ fluxes, Sci. Online Lett. Atmos., 7, 161-164, <https://doi.org/10.2151/sola.2011-041>, 2011.
- Takahashi, T., Sutherland, S. C., Wanninkhof, R., Sweeney, C., Feely, R. A., Chipman, D. W., Hales, B., Friederich, G., Chavez, F., Sabine, C., Watson, A., Bakker, D. C. E., Schuster, U., Metzl, N., Yoshikawa-Inoue, H., Ishii, M., Midorikawa, T., Nojiri, Y., Koertzinger, A., Steinhoff, T., Hoppe, M., Olafsson, J., Arnarson, T. S., Tilbrook, B., Johannessen, T., Olsen, A., Bellerby, R., Wong, C. S., Delille, B., Bates, N. R., and de Baar, H. J. W.: Climatological mean and decadal change in surface ocean pCO₂, and net sea-air CO₂ flux over the global oceans, Deep-Sea Res. Pt. II, 56, 554-577, <https://doi.org/10.1016/j.dsr2.2008.12.009>, 2009.
- 695 Té, Y., Jeseck, P., and Janssen, C.: TCCON data from Paris (FR), Release GGG2020.R0 (R0) [dataset], <https://doi.org/10.14291/tcon.ggg2020.paris01.R0>, 2014.
- 700 Tian, X. and Feng, X.: A non-linear least squares enhanced POD-4DVar algorithm for data assimilation, Tellus A, 67, 25340, <https://doi.org/10.3402/tellusa.v67.25340>, 2015.
- Tian, X., Zhang, H., Feng, X., and Xie, Y.: Nonlinear least squares En4DVar to 4DEnVar methods for data assimilation: Formulation, analysis, and preliminary evaluation, Mon. Weather Rev., 146, 77-93, <https://doi.org/10.1175/mwr-d-17-0050.1>, 2018.
- 705 van der Velde, I. R., van der Werf, G. R., Houweling, S., Maasakkers, J. D., Borsdorff, T., Landgraf, J., Tol, P., van Kempen, T. A., van Hees, R., Hoogeveen, R., Veefkind, J. P., and Aben, I.: Vast CO₂ release from Australian fires in 2019–2020 constrained by satellite, Nature, 597, 366-369, <https://doi.org/10.1038/s41586-021-03712-y>, 2021.
- 710 van der Werf, G. R., Randerson, J. T., Giglio, L., van Leeuwen, T. T., Chen, Y., Rogers, B. M., Mu, M., van Marle, M. J. E., Morton, D. C., Collatz, G. J., Yokelson, R. J., and Kasibhatla, P. S.: Global fire emissions estimates during 1997–2016, Earth Syst. Sci. Data, 9, 697-720, <https://doi.org/10.5194/essd-9-697-2017>, 2017.
- Wang, H., Jiang, F., Wang, J., Ju, W., and Chen, J. M.: Terrestrial ecosystem carbon flux estimated using GOSAT and OCO-2 XCO₂ retrievals, Atmos. Chem. Phys., 19, 12067-12082, <https://doi.org/10.5194/acp-19-12067-2019>, 2019.
- 715 Wang, J., Feng, L., Palmer, P. I., Liu, Y., Fang, S., Bösch, H., O'Dell, C. W., Tang, X., Yang, D., Liu, L., and Xia, C.: Large Chinese land carbon sink estimated from atmospheric carbon dioxide data, Nature, 586, 720-723, <https://doi.org/10.1038/s41586-020-2849-9>, 2020.
- 720 Wang, W., Ciais, P., Nemani, R. R., Canadell, J. G., Piao, S., Sitch, S., White, M. A., Hashimoto, H., Milesi, C., and Myneni, R. B.: Variations in atmospheric CO₂ growth rates coupled with tropical temperature, P. Natl. Acad. Sci. USA, 110, 13061-13066, <https://doi.org/10.1073/pnas.1219683110>, 2013.
- 725 Wang, Y., Tian, X., Chevallier, F., Johnson, M. S., Philip, S., Baker, D. F., Schuh, A. E., Deng, F., Zhang, X., Zhang, L., Zhu, D., and Wang, X.: Constraining China's land carbon sink from emerging satellite CO₂ observations: Progress and challenges, Glob. Change Biol., 28, 6838-6846, <https://doi.org/10.1111/gcb.16412>, 2022a.
- 730 Wennberg, P. O., Wang, X., Wang, K., Chevallier, F., Zhu, D., Lian, J., He, Y., Tian, H., Li, J., Zhu, J., Jeong, S., and Canadell, J. G.: The size of the land carbon sink in China, Nature, 603, E7-E9, <https://doi.org/10.1038/s41586-021-04255-y>, 2022b.
- 735 Warneke, T., Petri, C., Notholt, J., and Buschmann, M.: TCCON data from Orléans (FR), Release GGG2020.R0 (R0) [dataset], <https://doi.org/10.14291/tcon.ggg2020.orleans01.R0>, 2022.
- Weidmann, D., Brownsword, R., and Doniki, S.: TCCON data from Harwell, Oxfordshire (UK), Release GGG2020.R0 (R0) [dataset], <https://doi.org/10.14291/tcon.ggg2020.harwell01.R0>, 2023.
- 740 Wennberg, P. O., Roehl, C. M., Blavier, J.-F., Wunch, D., and Allen, N. T.: TCCON data from Jet Propulsion Laboratory (US), 2011, Release GGG2020.R0 (R0) [dataset], <https://doi.org/10.14291/TCCON.GGG2014.JPL02.R1/1330096>, 2022a.
- Wennberg, P. O., Wunch, D., Roehl, C. M., Blavier, J.-F., Toon, G. C., and Allen, N. T.: TCCON data from Lamont (US), Release GGG2020.R0 (R0) [dataset], <https://doi.org/10.14291/TCCON.GGG2014.LAMONT01.R1/1255070>, 2022b.
- Wennberg, P. O., Roehl, C. M., Wunch, D., Blavier, J.-F., Toon, G. C., Allen, N. T., Treffers, R., and Laughner, J.: TCCON data from Caltech (US), Release GGG2020.R0 (R0) [dataset], <https://doi.org/10.14291/TCCON.GGG2014.PASADENA01.R1/1182415>, 2022c.
- 745 Wennberg, P. O., Roehl, C. M., Wunch, D., Toon, G. C., Blavier, J.-F., Washenfelder, R., Keppel-Aleks, G., and Allen, N. T.: TCCON data from Park Falls (US), Release GGG2020.R1 (R1) [dataset], <https://doi.org/10.14291/tcon.ggg2020.parkfalls01.R1>, 2022d.
- Wu, M., Scholze, M., Kaminski, T., Vossbeck, M., and Tagesson, T.: Using SMOS soil moisture data combining CO₂ flask samples to constrain carbon fluxes during 2010-2015 within a Carbon Cycle Data Assimilation System (CCDAS), Remote Sens. Environ., 240, <https://doi.org/10.1016/j.rse.2020.111719>, 2020.
- Wunch, D., Toon, G. C., Sherlock, V., Deutscher, N. M., Liu, X., Feist, D. G., and Wennberg, P. O.: The Total Carbon Column Observing Network's GGG2014 Data Version [dataset], <https://doi.org/10.14291/tcon.ggg2014.documentation.R0/1221662>, 2015.
- 750 Wunch, D., Toon, G. C., Blavier, J.-F. L., Washenfelder, R. A., Notholt, J., Connor, B. J., Griffith, D. W., Sherlock, V., and Wennberg, P. O.: The Total Carbon Column Observing Network, Philos. T. R. Soc. A, 369, 2087-2112, <https://doi.org/10.1098/rsta.2010.0240>, 2011.



- 745 Wunch, D., Mendonca, J., Colebatch, O., Allen, N. T., Blavier, J.-F., Kunz, K., Roche, S., Hedelius, J., Neufeld, G., Springett, S., Worthy, D., Kessler, R., and Strong, K.: TCCON data from East Trout Lake, SK (CA), Release GGG2020.R0 (R0) [dataset], <https://doi.org/10.14291/tcon.ggg2020.easttroutlake01.R0>, 2022.
- Wunch, D., Wennberg, P. O., Osterman, G., Fisher, B., Naylor, B., Roehl, C. M., O'Dell, C., Mandrake, L., Viatte, C., Kiel, M., Griffith, D. W. T., Deutscher, N. M., and Velazco, V. A.: Comparisons of the Orbiting Carbon Observatory-2 (OCO-2) XCO₂ measurements with TCCON, *Atmos. Meas. Tech.*, 10, 2209-2238, <https://doi.org/10.5194/amt-10-2209-2017>, 2017.
- 750 Yokota, T., Yoshida, Y., Eguchi, N., Ota, Y., Tanaka, T., Watanabe, H., and Maksyutov, S.: Global concentrations of CO₂ and CH₄ retrieved from GOSAT: First preliminary results, *Sci. Online Lett. Atmos.*, 5, 160-163, <https://doi.org/10.2151/sola.2009-041>, 2009.
- Zeng, N., Mariotti, A., and Wetzel, P.: Terrestrial mechanisms of interannual CO₂ variability, *Global Biogeochem. Cy.*, 19, GB1016, <https://doi.org/10.1029/2004gb002273>, 2005.
- 755 Zhang, Q., Shia, R.-L., Sander, S. P., and Yung, Y. L.: XCO₂ retrieval error over deserts near critical surface albedo, *Earth Space Sci.*, 3, 36-45, <https://doi.org/10.1002/2015EA000143>, 2016.
- Zhou, M., Wang, P., Kumps, N., Hermans, C., and Nan, W.: TCCON data from Xianghe, China, Release GGG2020.R0 (R0) [dataset], <https://doi.org/10.14291/tcon.ggg2020.xianghe01.R0>, 2022.
- 760 Zscheischler, J., Mahecha, M. D., Avitabile, V., Calle, L., Carvalhais, N., Ciais, P., Gans, F., Gruber, N., Hartmann, J., Herold, M., Ichii, K., Jung, M., Landschutzer, P., Laruelle, G. G., Lauerwald, R., Papale, D., Peylin, P., Poulter, B., Ray, D., Regnier, P., Rodenbeck, C., Roman-Cuesta, R. M., Schwalm, C., Tramontana, G., Tyukavina, A., Valentini, R., van der Werf, G., West, T. O., Wolf, J. E., and Reichstein, M.: Reviews and syntheses: An empirical spatiotemporal description of the global surface-atmosphere carbon fluxes: opportunities and data limitations, *Biogeosciences*, 14, 3685-3703, <https://doi.org/10.5194/bg-14-3685-2017>, 2017.